Steel and Composite Structures, *Vol. 28, No. 3 (2018) 331-347*
DOI: https://doi.org/10.12989/scs.2018.28.3.331

Creep analysis of the FG cylinders: Time-dependent non-axisymmetric behavior

Mohammad Arefi *, Mehrdad Nasr and Abbas Loghman

Department of Solid Mechanics, Faculty of Mechanical Engineering, University of Kashan, Kashan, Iran

(*Received January 4, 2018, Revised May 15, 2018, Accepted June 2, 2018*)

Abstract. In this paper history of stresses, strains, radial and circumferential displacements of a functionally graded thick-walled hollow cylinder due to creep phenomenon is investigated. The cylinder is subjected to an arbitrary non-axisymmetric two dimensional thermo-mechanical loading and uniform magnetic field along axial direction. Using equilibrium, strain-displacements and stress-strain relations, the governing differential equations of the problem containing creep strains are derived in terms of radial and circumferential displacements. Since the displacements are varying with time due to creep phenomenon, an analytical solution is not available for these equations. Thus, a semi-analytical procedure based on separation of variables and Fourier series together with a numerical procedure is employed. The numerical results indicate that the non-axisymmetric loading and the material grading index have significant effect on stress redistributions. Moreover, by proper selection of material for any combination of non-axisymmetric loading, one can arrive suitable response for the cylinder to achieve optimal design. With some simplifications, the results are validated with the existing literature.

Keywords: FGM hollow cylinder; time dependent creep; non-axisymmetric; two-dimensional loads

1. Introduction

Functionally graded materials (FGMs) which contain continuous and gradual changes in composition, structure and properties in different directions are intensively investigated in recent years. For most of these materials, the properties are assumed to obey the power law, non-linear or exponential patterns. Design process of such materials requires accurate structural analysis. For this reason, analysis of structures made of FGM and similar composites with variable properties has been an active area of research in the past two decades

Jabbari *et al*. (2003) presented a general thermoelastic solution of a functionally graded hollow cylinder under non-axisymmetric thermal and mechanical loads. They used the separation of variables and complex Fourier series to solve the governing equations. One can find that the proposed method was applicable for special boundary conditions. Shao *et al*. (2008) studied non-axisymmetric thermo-mechanical behavior of functionally graded hollow cylinders subjected to transient heat conduction and mechanical loads. They employed Laplace transformations and complex Fourier series in their analysis. The obtained results lead to a steady state case when time approaches to infinity.

In another research, asymmetric transient thermal and mechanical loads were applied to a hollow FGM cylinder in which separation of variable method and Bessel function were used to derive constitutive equations (Jabbari *et al*. 2008). Functionally graded hollow spheres subjected to non-axisymmetric loads were analyzed by Poultangari *et al*. (2008). The Legendre polynomials and Euler differential equations were used to solve the problem. Fesharaki *et al*. (2012) investigated the effects of electrical fields as well as thermal and mechanical loadings on the non-axisymmetric behavior of a hollow cylinder made of functionally graded piezoelectric materials (FGPM). Ootao and Ishihara (2013) studied the asymmetric transient thermal stresses of a functionally graded hollow cylinder. They presented an exact solution and demonstrated the effect of functionally grading index on thermal stress distributions. Elastic analysis of an infinite length FGM cylinder under arbitrary non-uniform mechanical loadings was studied by Li and Liu (2014). Sahan (2015) presented an alternative analytical method for transient vibration analysis of doubly-curved laminated shells subjected to dynamic loads. The cylinder was divided into some finite sub cylinders and the continuity conditions were applied between the layers. The obtained results showed that the effect of non-symmetric pressure is very important and significantly changes the stress distribution. Arani *et al*. (2015) studied non-axisymmetric behavior of a composite cylinder reinforced by carbon nano-tube under thermo-mechanical and uniform electro-magnetic loadings. They examined two dimensional elastic stress distribution using Mori-Tanaka theory. The effect of magnetic field and inhomogeneity on the non-axisymmetric thermo mechanical response of a FG cylinder was studied by Loghman *et al*. (2017). They showed that employing suitable magnetic field and inhomogeneity index can enhance thermoelastic response of such vessels. Free vibration analysis of micro and nanobeam subjected to magneto-electric loads was studied by Arefi and Zenkour

*Corresponding author, Assistant Professor,
E-mail: arefi63@gmail.com; arefi@kashanu.ac.ir

http://www.techno-press.org/?journal=scs&subpage=6
ISSN: 1229-9367 (Print), 1598-6233 (Online)

(2016a, b). In addition, influence of magnetic loads as well as thermal and electrical loads was studied on the various structures (Arefi and Zenkour 2017a-i).

Although many researchers have studied elastic and thermo-elastic behavior of cylinders subjected to non-axisymmetric loadings but none of them have so far considered the time-dependent creep response of such cylinders. Loghman and Wahab (1996) studied creep damage in thick-walled tubes made of isotropic materials. Theta projection concept as well as Robinson's model was employed in their analysis. Yang (2000) investigated elastic and time-dependent creep behavior of the cylinder with a thin coating of functionally graded material. He obtained the constitutive differential equation in terms of displacement rate using the equations of equilibrium, compatibility, Norton's law and Prandtl-Reuss relations. Steady state creep in thick-walled FGM cylinder was carried out by You *et al*. (2007). They examined the effect of parameters involved in Norton's law on radial, circumferential and axial stresses. As a new research, Loghman *et al*. (2010) considered the effect of uniform magnetic and temperature fields on the time-dependent creep response of a FGM cylinder subjected to inner pressure. In this work the creep behavior of the thick-walled FGM cylinder was described by Norton's law. They found that the inhomogeneity parameter of the material has a significant influence on redistribution of circumferential and effective stresses. Time-dependent creep on a radially polarized piezoelectric cylinder developed by Arani *et al*. (2011). Electro-thermo-mechanical loads were considered for a PZT5 hollow cylinder. A semi-analytical and a successive elastic solution method were employed for solution of the governing differential equations of the system. Time-dependent creep analysis of a rotating disk made of functionally graded material was studied by Loghman *et al*. (2013). The disk was subjected to electro-thermo-magnetic loads and temperature gradient. Steady-state creep analysis of a FG rotating cylinder made of an aluminum matrix reinforced with silicon carbide particles has been studied by Mangal *et al*. (2013). They showed that influence of silicon carbide particles on stress components is considerable. Using Norton's creep law, Nejad and Kashkoli (2014), investigated the effect of heat flux on time dependent creep of a rotating FGM hollow cylinder. They determined stresses at any time iteratively and their results was presented for different values of pressure and Norton's power law exponent. Golmakaniyoon and Akhlaghi (2016) performed time-dependent steady state creep modeling of FGM beams under thermal loading using successive approximation method. In addition, some time-dependent creep analysis for different materials and geometries based on mathematical and experimental analyses were presented by the references (Gallo *et al*. 2016, Brnic *et al*. 2016, Ginder *et al*. 2018).

Time-dependent creep analysis is necessary for the life assessment of structures subjected to various types of loading operating at high temperatures. The creep analysis gives the history of stresses and strains which can be used to damage analysis and predict the remnant life of the structure. A review of literature indicates that the time dependent creep analysis of a functionally graded cylinder subjected to non-axisymmetric thermal and mechanical loadings is not yet considered. In this work, a semi-analytical approach based on separation of variables and Fourier series together with a numerical procedure is employed to obtain history of stresses, strains, radial and circumferential displacements in a cylinder subjected to non-axisymmetric thermomechanical loadings and uniform magnetic field. The effect of material grading index, magnetic intensity and thermomechanical loadings is investigated on the responses.

2. Geometry, loading and material properties

An FGM hollow cylinder with inner and outer radii (a, b) is considered. Non-axisymmetric thermo-mechanical loadings and uniform magnetic field $\vec{H}(0,0,H_z)$ are applied on the cylinder as shown in Fig. 1. The origin of cylindrical coordinate system is located at the center of the cylinder.

All mechanical, thermal and magnetic properties except Poisson's ratio are assumed to be variable along the radial direction based on the power law variation as (Arefi and Rahimi 2011a, b, 2012a, b, c, d, Rahimi *et al*. 2012, 2014a, b, Arefi *et al*. 2012, 2017, Arefi and Nahas 2014, Arefi 2014, 2015, 2016a, b, Arefi and Allam 2015, Zenkour and Arefi 2017, Loghman *et al*. 2017, 2018).

$$\begin{aligned} E(r) &= E_i\left(r/a\right)^{\beta_1} \quad , \quad \alpha(r) = \alpha_i\left(r/a\right)^{\beta_2} \\ K(r) &= K_i\left(r/a\right)^{\beta_3} \quad , \quad \mu(r) = \mu_i\left(r/a\right)^{\beta_4} \end{aligned} \tag{1}$$

In which, E_i, α_i, K_i, μ_i are Young's modulus, coefficient of thermal expansion, thermal conductivity and magnetic permeability at the inner radius respectively. Also β_i (i = 1,

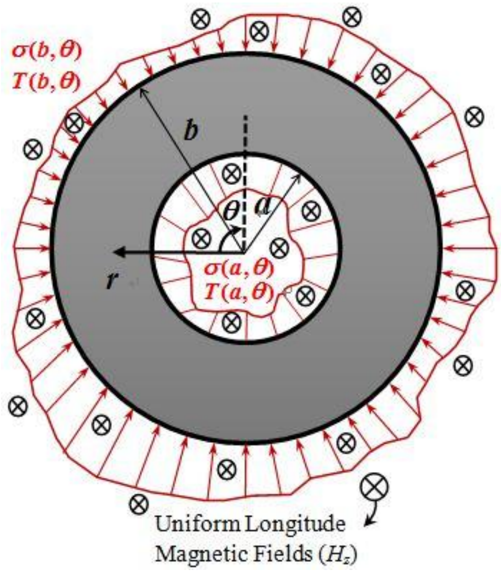

Fig. 1 The schematic of hollow FGM cylinder under non-axisymmetric thermo-mechanical loads and uniform longitudinal magnetic fields

2, 3, 4) are material in-homogeneity parameters. The material creep constitutive model obeys the Norton's power law, $\dot{\varepsilon}_e^c = B(r)\sigma_e^{n(r)}$, in which $\dot{\varepsilon}_e^c$, σ_e are the effective creep strain rate and the effective stress. $B(r)$ and $n(r)$ are the material creep parameters which must be obtained by experiment for different materials (Loghman *et al*. 2010). In this paper $B(r) = b_0 r^{b1}$ and $n(r)$ is considered to be a constant $n(r) = n_0$.

3. Governing equations

In this section, the fundamental relations for time-dependent creep analysis of a hollow FGM cylinder under two-dimensional thermo-mechanical loadings and uniform magnetic field are presented. For a non-axisymmetric problem under plane strain condition, the strain-displacement relations using radial and circumferential displacement components are written as (Sadd 2009)

$$\begin{aligned} \varepsilon_r &= \frac{\partial u}{\partial r} \\ \varepsilon_\theta &= \frac{1}{r}\left(\frac{\partial v}{\partial \theta} + u\right) \\ \varepsilon_{r\theta} &= \frac{1}{2}\left(\frac{1}{r}\frac{\partial u}{\partial \theta} + \frac{\partial v}{\partial r} - \frac{v}{r}\right) \end{aligned} \tag{2}$$

Where, u and v are the radial and circumferential displacements respectively. using the constitutive relations $\sigma_{ij} = \lambda(\varepsilon_{kk} - \varepsilon_{kk}^c)\delta_{ij} + 2G(\varepsilon_{ij} - \varepsilon_{ij}^c) - (3\lambda + 2G)\alpha\Delta T\delta_{ij}$ for a structures subjected to thermal loads, the stress components can be derived as follows (Mendelson 1968, Penney and Marriott 1971)

$$\begin{aligned} \sigma_r &= (\lambda + 2G)\left(\frac{\partial u}{\partial r} - \varepsilon_r^c\right) + \lambda\left(\frac{1}{r}\frac{\partial v}{\partial \theta} + \frac{u}{r} - \varepsilon_\theta^c\right) \\ &\quad -(3\lambda + 2G)\alpha T(r,\theta) \\ \sigma_\theta &= (\lambda + 2G)\left(\frac{1}{r}\frac{\partial v}{\partial \theta} + \frac{u}{r} - \varepsilon_\theta^c\right) + \lambda\left(\frac{\partial u}{\partial r} - \varepsilon_r^c\right) \\ &\quad -(3\lambda + 2G)\alpha T(r,\theta) \\ \sigma_{r\theta} &= G\left(\frac{1}{r}\frac{\partial u}{\partial \theta} + \frac{\partial v}{\partial r} - \frac{v}{r} - 2\varepsilon_{r\theta}^c\right) \end{aligned} \tag{3}$$

In which, σ_{ij}, ε_{ij} and ε_j^c (i, j = r, θ, z) are stress, total strain and creep strain tensors respectively, ΔT is temperature gradient with respect to reference temperature (T_0), λ is Lamé's constant, δ_{ij} is the Kronecker delta and G is the shear modulus of the material. λ, G are expressed in terms of Modulus of elasticity (E) and Poisson's ratio (υ). The equilibrium equations in cylindrical coordinates with considering body forces are written as follows

$$\begin{aligned} &\frac{\partial \sigma_r}{\partial r} + \frac{1}{r}\frac{\partial \sigma_{r\theta}}{\partial \theta} + \frac{\sigma_r - \sigma_\theta}{r} + f_r = 0 \\ &\frac{\partial \sigma_{r\theta}}{\partial r} + \frac{1}{r}\frac{\partial \sigma_\theta}{\partial \theta} + \frac{2}{r}\sigma_{r\theta} + f_\theta = 0 \end{aligned} \tag{4}$$

In which, f_r and f_θ are the Lorentz's force components in radial and circumferential directions.

The Lorentz's force is produced under the effect of magnetic field mentioned by the governing electrodynamics Maxwell equations as (Arefi *et al*. 2011, Firouz-Abadi *et al*. 2014)

$$\begin{aligned} &\vec{h} = curl(\vec{U} \times \vec{H}), \quad \nabla.\vec{h} = 0, \quad \vec{e} = -\mu(\frac{\partial \vec{U}}{\partial t} \times \vec{H}) \\ &\vec{j} = curl(\vec{h}), \quad curl(\vec{e}) = -\mu\frac{\partial \vec{h}}{\partial t}, \quad \vec{f} = \mu(\vec{j} \times \vec{H}) \end{aligned} \tag{5}$$

In which $\vec{h}$, $\vec{U}$, $\vec{H}$, $\vec{e}$, μ, $\vec{j}$ and $\vec{f}$ are perturbation of magnetic field vector, displacement vector, magnetic vector, perturbation of electric field vector, magnetic permeability, electric current density vector and Lorentz's force vector.

Imposing a uniform longitudinal magnetic field $\vec{H}(0,0,H_z)$ in axial direction, the Lorentz's force components in terms of radial and circumferential displacements are written as

$$\begin{aligned} f_r &= \mu_i r^{\beta_4} H_z^2 \frac{\partial}{\partial r}\left(\frac{\partial u}{\partial r} + \frac{u}{r} + \frac{1}{r}\frac{\partial v}{\partial \theta}\right) \\ f_\theta &= \mu_i r^{\beta_4} H_z^2 \frac{1}{r}\frac{\partial}{\partial \theta}\left(\frac{\partial u}{\partial r} + \frac{u}{r} + \frac{1}{r}\frac{\partial v}{\partial \theta}\right) \end{aligned} \tag{6}$$

Substituting Eq. (3) into Equilibrium Eq. (4) and considering the Lorentz's force components Eq. (6) leads to the governing differential equations in terms of displacements containing creep strains as shown

$$\begin{aligned} &\frac{\partial^2 u}{\partial r^2} + \frac{s_1}{r}\frac{\partial u}{\partial r} + \frac{s_2}{r^2}u + \frac{s_3}{r^2}\frac{\partial^2 u}{\partial \theta^2} + \frac{s_4}{r}\frac{\partial^2 v}{\partial r \partial \theta} + \frac{s_5}{r^2}\frac{\partial v}{\partial \theta} \\ &= s_6 r^{\beta_2 - 1}T + s_7 r^{\beta_2}\frac{\partial T}{\partial r} + \frac{s_8}{r}\varepsilon_r^c + \frac{s_9}{r}\varepsilon_\theta^c \\ &\quad + s_{10}\frac{\partial \varepsilon_r^c}{\partial r} + s_{11}\frac{\partial \varepsilon_\theta^c}{\partial r} + \frac{s_{12}}{r}\frac{\partial \varepsilon_{r\theta}^c}{\partial \theta} \\ &\frac{\partial^2 v}{\partial r^2} + \frac{s_{13}}{r}\frac{\partial v}{\partial r} + \frac{s_{14}}{r^2}v + \frac{s_{15}}{r^2}\frac{\partial^2 v}{\partial \theta^2} + \frac{s_{16}}{r}\frac{\partial^2 u}{\partial r \partial \theta} + \frac{s_{17}}{r^2}\frac{\partial u}{\partial \theta} \\ &= s_{18} r^{\beta_2 - 1}\frac{\partial T}{\partial \theta} + \frac{s_{19}}{r}\varepsilon_{r\theta}^c + s_{20}\frac{\partial \varepsilon_{r\theta}^c}{\partial r} + \frac{s_{21}}{r}\frac{\partial \varepsilon_r^c}{\partial \theta} + \frac{s_{22}}{r}\frac{\partial \varepsilon_\theta^c}{\partial \theta} \end{aligned} \tag{7}$$

In which β_4 is considered equal to β_1. In addition, the constants s_1 to s_{22} are given in Appendix A. Complex Fourier series for the radial and circumferential displacements, temperature distribution and creep strains are considered as $\Re(r,\theta) = \sum_{n=-\infty}^{+\infty}\Re_n(r)e^{in\theta}$ in which $\Re = u_n, v_n, T_n, \varepsilon_{r,n}^c, \varepsilon_{\theta,n}^c, \varepsilon_{r\theta,n}^c$ are the coefficients of the complex and n is number of terms (Lee and Fenner 1986, Jabbari *et al*. 2003). Substituting the assumed terms as complex series in to equilibrium relations yields

$$\begin{aligned} &\frac{\partial^2 u_n}{\partial r^2} + \frac{s_1}{r}\frac{\partial u_n}{\partial r} + \frac{s_2 - s_3 n^2}{r^2}u_n + in\frac{s_4}{r}\frac{\partial v_n}{\partial r} + in\frac{s_5}{r^2}v_n \\ &= s_6 r^{\beta_2 - 1}T_n + s_7 r^{\beta_2}\frac{\partial T_n}{\partial r} + \frac{s_8}{r}\varepsilon_{r,n}^c + \frac{s_9}{r}\varepsilon_{\theta,n}^c \end{aligned} \tag{8}$$

$$+s_{10}\frac{\partial \varepsilon^{c}_{r,n}}{\partial r}+s_{11}\frac{\partial \varepsilon^{c}_{\theta,n}}{\partial r}+in\frac{s_{12}}{r}\varepsilon^{c}_{r\theta,n}$$

$$\frac{\partial^2 v_n}{\partial r^2}+\frac{s_{13}}{r}\frac{\partial v_n}{\partial r}+\frac{s_{14}-s_{15}n^2}{r^2}v_n+in\frac{s_{16}}{r}\frac{\partial u_n}{\partial r}+in\frac{s_{17}}{r^2}u_n \tag{8}$$

$$=ins_{18}r^{\beta_2-1}T_n+\frac{s_{19}}{r}\varepsilon^{c}_{r\theta,n}+s_{20}\frac{\partial \varepsilon^{c}_{r\theta,n}}{\partial r}+in\frac{s_{21}}{r}\varepsilon^{c}_{r,n}+in\frac{s_{22}}{r}\varepsilon^{c}_{\theta,n}$$

4. Solution of the differential equation

4.1 Heat conduction problem

The steady state heat transfer equation without heat generation in cylindrical coordinate system of an FG cylinder is expressed (Jain and Singh 2009) as follows

$$\frac{\partial^2 T}{\partial r^2}+\left(\frac{1}{K}\frac{\partial K}{\partial r}+\frac{1}{r}\right)\frac{\partial T}{\partial r}+\frac{1}{r^2}\frac{\partial^2 T}{\partial \theta^2}=0 \qquad \begin{array}{c} a\le r\le b \\ -\pi\le\theta\le\pi \end{array} \tag{9}$$

Boundary condition of heat transfer equation are defined in general linear form (Jain and Singh 2009) which can be simplified for different types of conduction, convection and radiation processes or combination of them as

$$\begin{aligned}&\chi_{11}T(a,\theta)+\chi_{12}\frac{\partial T(a,\theta)}{\partial r}=F_1(\theta)\\ &\chi_{21}T(b,\theta)+\chi_{22}\frac{\partial T(b,\theta)}{\partial r}=F_2(\theta)\end{aligned} \tag{10}$$

χ_{ij} (i, j = 1, 2) are the constants depending on thermal conductivity and thermal convection coefficients. $F_1(\theta)$ and $F_2(\theta)$ are known arbitrary functions on the inner and outer radii, respectively. The steady state heat conduction problem is solved by the following solution (Hetnarski *et al*. 2009, Loghman *et al*. 2017).

$$\begin{aligned}&T(r,\theta)=\sum_{n=-\infty}^{\infty}T_n e^{in\theta}=\sum_{n=-\infty}^{\infty}\left(A_{n1}r^{\zeta_{n1}}+A_{n2}r^{\zeta_{n2}}\right)e^{in\theta}\\ &\zeta_{n1,2}=\frac{-\beta_3}{2}\pm\left(\frac{\beta_3^{\,2}}{4}+n^2\right)^{1/2}\end{aligned} \tag{11}$$

Where the unknown coefficients of A_{n1} and A_{n2} can be determined by thermal boundary conditions as presented in Appendix A.

4.2 Magneto-thermo-mechanical analysis of hollow cylinder

To investigate the thermo-elastic response of the cylinder, creep strains are ignored in Eq. (8). Substituting temperature distribution based on the Eq. (11) in Eq. (8), two governing differential equations of the system in terms of radial and circumferential displacements are derived as

$$\frac{\partial^2 u_n}{\partial r^2}+\frac{s_1}{r}\frac{\partial u_n}{\partial r}+\frac{s_2-s_3n^2}{r^2}u_n+in\left(\frac{s_4}{r}\frac{\partial v_n}{\partial r}+\frac{s_5}{r^2}v_n\right) \tag{12}$$

$$=(s_6+\zeta_{n1}s_7)A_{n1}r^{\beta_2+\zeta_{n1}-1}+(s_6+\zeta_{n2}s_7)A_{n2}r^{\beta_2+\zeta_{n2}-1}$$

$$\frac{\partial^2 v_n}{\partial r^2}+\frac{s_{13}}{r}\frac{\partial v_n}{\partial r}+\frac{s_{14}-s_{15}n^2}{r^2}v_n+in\left(\frac{s_{16}}{r}\frac{\partial u_n}{\partial r}+\frac{s_{17}}{r^2}u_n\right) \tag{12}$$

$$=ins_{18}(A_{n1}r^{\beta_2+\zeta_{n1}-1}+A_{n2}r^{\beta_2+\zeta_{n2}-1})$$

Eq. (12) are a system of non-homogeneous ordinary differential equations which have general and particular solutions. The general solution consists of two cases $n = 0$ and $n \neq 0$. The differential equations for $n = 0$ are uncoupled. The solution is obtained from sum of the general and particular solutions as

$$\begin{aligned}&u_n(r)=\left(u_0+u_{n,n\neq0}\right)^g+\left(u_0+u_{n,n\neq0}\right)^p\\ &v_n(r)=\left(v_0+v_{n,n\neq0}\right)^g+\left(v_0+v_{n,n\neq0}\right)^p\end{aligned} \tag{13}$$

(a) For $n \neq 0$

General homogeneous solution of the problem is considered as

$$u_n^g(r)=C\,r^{\gamma}\quad,\quad v_n^g(r)=D\,r^{\gamma} \tag{14}$$

where, C and D are constants which can be obtained from boundary conditions. Substituting Eq. (14) into Eq. (12), yields two algebraic equations for obtaining the constants C and D. The non-trivial solution of the problem is obtained by setting the determinant of the coefficient equal to zero. Equating the determinant to zero yields eigen-values of the problem (γ_{n1} to γ_{n4}) as

$$\begin{aligned}&u_n^g(r)=\sum_{j=1}^{4}C_{nj}\,r^{\gamma_{nj}}\\ &v_n^g(r)=\sum_{j=1}^{4}N_{nj}C_{nj}\,r^{\gamma_{nj}}\end{aligned} \tag{15}$$

In which N_{nj} is the relation between constants C_{nj}, D_{nj}.

$$N_{nj}=\frac{i\left[\gamma_{nj}(\gamma_{nj}-1)+s_1\gamma_{nj}+s_2-n^2s_3\right]}{n\left[s_4\gamma_{nj}+s_5\right]}\qquad j=1,2,3,4 \tag{16}$$

To derive the particular solution, considering the right hand side of Eq. (12) the polynomial functions are assumed as

$$\begin{aligned}&u^p_{n,n\neq0}(r)=G_{n1}\,r^{\psi_{n1}}+G_{n2}\,r^{\psi_{n2}}\\ &v^p_{n,n\neq0}(r)=G_{n3}\,r^{\psi_{n1}}+G_{n4}\,r^{\psi_{n2}}\\ &,\quad \psi_{ni}=\zeta_{ni}+\beta_2+1\quad(i=1,2)\end{aligned} \tag{17}$$

By substituting Eq. (17) into Eq. (12) and rearranging the terms with the same power, the unknown amplitudes defined in Eq. (17) are obtained as

$$G_{n1}=\frac{g_5g_7-g_3g_{11}}{g_1g_7-g_3g_9},\;G_{n2}=\frac{g_6g_8-g_4g_{12}}{g_2g_8-g_4g_{10}}, \tag{18}$$

$$G_{n3}=\frac{g_1g_{11}-g_5g_9}{g_1g_7-g_3g_9},\ G_{n4}=\frac{g_2g_{12}-g_6g_{10}}{g_2g_8-g_4g_{10}} \tag{18}$$

(b) For $n = 0$

In this case Eq. (12) is decoupled to ordinary differential equations containing the non-homogeneous and homogeneous Euler equations for radial and circumferential displacements, respectively which is solved as (Boyce *et al.* 1969)

$$\begin{aligned}&u_0(r)=\sum_{j=1}^{2}\left(C_{0j}r^{\gamma_{0j}}+G_{0j}r^{\psi_{0j}}\right),\\&\gamma_{0\,1,2}=\frac{-(s_1-1)\pm\sqrt{\Delta_1}}{2},\\&\Delta_1=(s_1-1)^2-4s_2\end{aligned} \tag{19}$$

$$\begin{aligned}&v_0(r)=\sum_{j=3}^{4}C_{0j}\,r^{\gamma_{0j}},\\&\gamma_{0\,3,4}=\frac{-(s_{13}-1)\pm\sqrt{\Delta_2}}{2},\\&\Delta_2=(s_{13}-1)^2-4s_{14}\end{aligned} \tag{20}$$

The terms $G_{0,j}$ of particular solution is derived by equating the same terms as follows

$$G_{0j}=\frac{s_6+s_7\zeta_{0j}}{\psi_{0j}(\psi_{0j}-1)+s_1\psi_{0j}+s_2}A_{0j}\qquad j=1,2 \tag{21}$$

By adding the obtained solutions for $n = 0$, $n \neq 0$ the general solution for $u(r, \theta)$ and $v(r, \theta)$ are expressed as

$$\begin{aligned}u(r,\theta)&=\sum_{j=1}^{2}\left(C_{0j}r^{\gamma_{0j}}+G_{0j}r^{\psi_{0j}}\right)\\&+\sum_{n=-\infty,n\neq0}^{n=\infty}\left[\sum_{j=1}^{4}C_{nj}\,r^{\gamma_{nj}}+G_{n1}\,r^{\psi_{n1}}+G_{n2}\,r^{\psi_{n2}}\right]e^{in\theta}\\v(r,\theta)&=\sum_{j=3}^{4}C_{0j}\,r^{\gamma_{0j}}\\&+\sum_{n=-\infty,n\neq0}^{n=\infty}\left[\sum_{j=1}^{4}N_{nj}C_{nj}\,r^{\gamma_{nj}}+G_{n3}\,r^{\psi_{n1}}+G_{n4}\,r^{\psi_{n2}}\right]e^{in\theta}\end{aligned} \tag{22}$$

Substituting Eq. (22) into Eq. (3) and ignoring creep strains, the stress components for elastic solution are obtained as

$$\begin{aligned}\sigma_r(r,\theta)&=\sum_{j=1}^{2}\left(K_1C_{0j}r^{\gamma_{0j}}+K_2r^{\psi_{0j}}\right)\\&\quad+\sum_{n=-\infty,n\neq0}^{n=\infty}\left[\sum_{j=1}^{4}K_3C_{nj}\,r^{\gamma_{nj}}+K_4r^{\psi_{n1}}+K_5\,r^{\psi_{n2}}\right]e^{in\theta}\\\sigma_\theta(r,\theta)&=\sum_{j=1}^{2}\left(K_6C_{0j}r^{\gamma_{0j}}+K_7r^{\psi_{0j}}\right)\\&\quad+\sum_{n=-\infty,n\neq0}^{n=\infty}\left[\sum_{j=1}^{4}K_8C_{nj}\,r^{\gamma_{nj}}+K_9r^{\psi_{n1}}+K_{10}\,r^{\psi_{n2}}\right]e^{in\theta}\\\sigma_{r\theta}(r,\theta)&=\sum_{j=3}^{4}K_{11}C_{0j}r^{\gamma_{0j}}\\&\quad+\sum_{n=-\infty,n\neq0}^{n=\infty}\left[\sum_{j=1}^{4}K_{12}C_{nj}\,r^{\gamma_{nj}}+K_{13}r^{\psi_{n1}}+K_{14}r^{\psi_{n2}}\right]e^{in\theta}\end{aligned} \tag{23}$$

Where the constants K_1 to K_{14} are given in the Appendix A. There are four unknown constants C_{nj} (j = 1, 2, 3, 4) in the stress and displacement relations which must be determined using four boundary conditions for displacements or stresses at the inner and outer radii. Expanding the given boundary conditions in complex Fourier series gives

$$\omega_j\left(\theta\right)=\sum_{n=-\infty}^{n=\infty}W_j(n)\,e^{in\theta}\qquad j=1,2,3,4 \tag{24}$$

Where

$$W_j(n)=\frac{1}{2\pi}\int_{-\pi}^{\pi}\omega_j\left(n\right)e^{-in\theta}d\theta\qquad j=1,2,3,4 \tag{25}$$

4.3 Time-dependent magneto-thermo-mechanical creep behavior of hollow cylinder

As mentioned previously, the creep strains are depending on the time, temperature and current stresses. The well-known Prandtl-Reuss equations demonstrate the relationship between the creep strain rates, effective stress, current stresses and creep behavior of the material. In cylindrical coordinate system these relations are expressed as (Mendelson 1968)

$$\begin{aligned}\dot{\varepsilon}_r^c&=\frac{\dot{\varepsilon}_e^c}{\sigma_e}\left(\sigma_r-\frac{\sigma_\theta+\sigma_z}{2}\right)\\\dot{\varepsilon}_\theta^c&=\frac{\dot{\varepsilon}_e^c}{\sigma_e}\left(\sigma_\theta-\frac{\sigma_r+\sigma_z}{2}\right)\\\dot{\varepsilon}_{r\theta}^c&=\frac{3\dot{\varepsilon}_e^c}{2\sigma_e}\sigma_{r\theta}\end{aligned} \tag{26}$$

In which, effective Von Mises stress is defined as follows

$$\begin{aligned}\sigma_e&=\frac{1}{\sqrt{2}}\sqrt{\left(\sigma_\theta-\sigma_r\right)^2+\left(\sigma_\theta-\sigma_z\right)^2+\left(\sigma_z-\sigma_r\right)^2+6\sigma_{r\theta}{}^2}\\&=\frac{\sqrt{3}}{2}\left[\left(\sigma_\theta-\sigma_r\right)^2+4\sigma_{r\theta}{}^2\right]^{0.5}\end{aligned} \tag{27}$$

Considering the plane-strain case, the axial strain component is considered to be zero and consequently based on the Norton's law, the Prandtl-Reuss equations are simplified as follows

$$\begin{aligned}\dot{\varepsilon}_r^c&=\frac{3}{4}B(r)\sigma_e^{\,n_0-1}\left(\sigma_r-\sigma_\theta\right)\\\dot{\varepsilon}_\theta^c&=\frac{3}{4}B(r)\sigma_e^{\,n_0-1}\left(\sigma_\theta-\sigma_r\right)\\\dot{\varepsilon}_{r\theta}^c&=\frac{3}{2}B(r)\sigma_e^{\,n_0-1}\sigma_{r\theta}\end{aligned} \tag{28}$$

Considering Eq. (8) in the rate form and substituting Prandtl-Reuss Eq. (28) the following time dependent differential equations are obtained

$$\begin{aligned}
&\frac{\partial^2 \dot{u}_n}{\partial r^2}+\frac{s_1}{r}\frac{\partial \dot{u}_n}{\partial r}+\frac{s_2-s_3 n^2}{r^2}\dot{u}_n+in\left(\frac{s_4}{r}\frac{\partial \dot{v}_n}{\partial r}+\frac{s_5}{r^2}\dot{v}_n\right)\\
&=\left[q_1+q_2+\frac{q_3+q_4}{r}\right]\sigma_e^{n_0-1}r^{b_1}\\
&\frac{\partial^2 \dot{v}_n}{\partial r^2}+\frac{s_{13}}{r}\frac{\partial \dot{v}_n}{\partial r}+\frac{s_{14}-s_{15} n^2}{r^2}\dot{v}_n+in\left(\frac{s_{16}}{r}\frac{\partial \dot{u}_n}{\partial r}+\frac{s_{17}}{r^2}\dot{u}_n\right)\\
&=\left[q_5+q_6+\frac{q_7+q_8}{r}\right]\sigma_e^{n_0-1}r^{b_1}
\end{aligned} \tag{29}$$

Where q_1 to q_8 are variables given in Appendix B. Eqs. (29) are a system of ordinary differential non-homogeneous equations which their general and particular solutions are assumed similar to thermo-elastic solution procedure. Hence homogeneous and particular solution of Eqs. (29) in case $n \neq 0$ is presented as

$$\dot{u}^g_{n,n\neq 0}(r)=\sum_{j=1}^{4}C_{nj}r^{\gamma_{nj}} \quad , \quad \dot{v}^g_{n,n\neq 0}(r)=\sum_{j=1}^{4}N_{nj}C_{nj}r^{\gamma_{nj}} \tag{30}$$

$$\begin{aligned}
\dot{u}^p_{n,n\neq 0}(r)&=H_{n1}r^{b_1+2}+H_{n2}r^{b_1+1},\\
\dot{v}^p_{n,n\neq 0}(r)&=H_{n3}r^{b_1+2}+H_{n4}r^{b_1+1}
\end{aligned} \tag{31}$$

Substituting Eq. (31) into Eq. (29) yields H_{n1} to H_{n4} as follows

$$\begin{aligned}
H_{n1}&=\frac{h_5h_7-h_3h_{11}}{h_1h_7-h_3h_9} \quad H_{n2}=\frac{h_6h_8-h_4h_{12}}{h_2h_8-h_4h_{10}}\\
H_{n3}&=\frac{h_1h_{11}-h_5h_9}{h_1h_7-h_3h_9} \quad H_{n4}=\frac{h_2h_{12}-h_6h_{10}}{h_2h_8-h_4h_{10}}
\end{aligned} \tag{32}$$

Where the parameters h_1 to h_{12} are written in Appendix B.

In case $n = 0$, the Eq. (29) are decoupled to ordinary differential equations as

$$\begin{aligned}
&\frac{\partial^2 \dot{u}_0}{\partial r^2}+\frac{s_1}{r}\frac{\partial \dot{u}_0}{\partial r}+\frac{s_2}{r^2}\dot{u}_0=\underbrace{\left(q_1+q_2+\frac{q_3+q_4}{r}\right)\sigma_e^{n_0-1}r^{b_1}}_{Q_1(r)}\\
&\frac{\partial^2 \dot{v}_0}{\partial r^2}+\frac{s_{13}}{r}\frac{\partial \dot{v}_0}{\partial r}+\frac{s_{14}}{r^2}\dot{v}_0=\underbrace{\left(q_5+q_6+\frac{q_7+q_8}{r}\right)\sigma_e^{n_0-1}r^{b_1}}_{Q_2(r)}
\end{aligned} \tag{33}$$

The homogeneous solution of Eq. (33) is derived as

$$\begin{aligned}
\dot{u}^g_0(r)&=\sum_{j=1}^{2}C_{0j}r^{\gamma_{0j}}=C_{01}\underbrace{r^{\gamma_{01}}}_{\dot{u}_0^{g_1}}+C_{02}\underbrace{r^{\gamma_{02}}}_{\dot{u}_0^{g_2}}\\
\dot{v}^g_0(r)&=\sum_{j=3}^{4}C_{0j}r^{\gamma_{0j}}=C_{03}\underbrace{r^{\gamma_{03}}}_{\dot{v}_0^{g_1}}+C_{04}\underbrace{r^{\gamma_{04}}}_{\dot{v}_0^{g_2}}
\end{aligned} \tag{34}$$

To obtain particular solutions, as mentioned at the beginning of the previous section, coefficients on the right hand side of the governing equations are not constant, so method of variation of parameters has been employed in this regard (Rice and Do 2012). This method is based on the premise that the particular solutions are linearly independent general solutions, therefore, particular solutions are assumed as

$$\begin{aligned}
\dot{u}^p_0(r)&=P_{01}\dot{u}_0^{g_1}+P_{02}\dot{u}_0^{g_2}=\sum_{j=1}^{2}P_{0j}r^{\gamma_{0j}}\\
\dot{v}^p_0(r)&=P_{03}\dot{v}_0^{g_1}+P_{04}\dot{v}_0^{g_2}=\sum_{j=3}^{4}P_{0j}r^{\gamma_{0j}}
\end{aligned} \tag{35}$$

Where the unknown functions $p_{0,j}$ (j = 1, 2, 3, 4) are obtained as

$$\begin{aligned}
P_{01}&=-\int\frac{\dot{u}_0^{g_2}Q_1(r)}{W(\dot{u}_0^{g_1},\dot{u}_0^{g_2})}dr \quad , \quad P_{02}=\int\frac{\dot{u}_0^{g_1}Q_1(r)}{W(\dot{u}_0^{g_1},\dot{u}_0^{g_2})}dr\\
P_{03}&=-\int\frac{\dot{v}_0^{g_2}Q_2(r)}{W(\dot{v}_0^{g_1},\dot{v}_0^{g_2})}dr \quad , \quad P_{04}=\int\frac{\dot{v}_0^{g_1}Q_2(r)}{W(\dot{v}_0^{g_1},\dot{v}_0^{g_2})}dr
\end{aligned} \tag{36}$$

We need to point out that in Eqs. (36) $W(\dot{u}_0^{g_1},\dot{u}_0^{g_2})$ and $W(\dot{v}_0^{g_1},\dot{v}_0^{g_2})$ are defined as

$$\begin{aligned}
W\left(\dot{u}_0^{g_1},\dot{u}_0^{g_2}\right)&=\begin{vmatrix}\dot{u}_0^{g_1} & \dot{u}_0^{g_2}\\ \frac{d\dot{u}_0^{g_1}}{dr} & \frac{d\dot{u}_0^{g_2}}{dr}\end{vmatrix}=\dot{u}_0^{g_1}\frac{d\dot{u}_0^{g_2}}{dr}-\frac{d\dot{u}_0^{g_1}}{dr}\dot{u}_0^{g_2}\\
W\left(\dot{v}_0^{g_1},\dot{v}_0^{g_2}\right)&=\begin{vmatrix}\dot{v}_0^{g_1} & \dot{v}_0^{g_2}\\ \frac{d\dot{v}_0^{g_1}}{dr} & \frac{d\dot{v}_0^{g_2}}{dr}\end{vmatrix}=\dot{v}_0^{g_1}\frac{d\dot{v}_0^{g_2}}{dr}-\frac{d\dot{v}_0^{g_1}}{dr}\dot{v}_0^{g_2}
\end{aligned} \tag{37}$$

With combining Eqs. (30)-(37) one can obtain the complete solution of Eqs. (29) as

$$\begin{aligned}
\dot{u}_n(r)&=\left(\dot{u}_0^g+\dot{u}^g_{n,n\neq 0}\right)+\left(\dot{u}_0^p+\dot{u}^p_{n,n\neq 0}\right)\\
&=\sum_{j=1}^{2}\left(C_{0j}+P_{0j}\right)r^{\gamma_{0j}}+\sum_{j=1}^{4}C_{nj}r^{\gamma_{nj}}+H_{n1}r^{b_1+2}+H_{n2}r^{b_1+1}\\
\dot{v}_n(r)&=\left(\dot{v}_0^g+\dot{v}^g_{n,n\neq 0}\right)+\left(\dot{v}_0^p+\dot{v}^p_{n,n\neq 0}\right)\\
&=\sum_{j=3}^{4}\left(C_{0j}+P_{0j}\right)r^{\gamma_{0j}}+\sum_{j=1}^{4}N_{nj}C_{nj}r^{\gamma_{nj}}+H_{n3}r^{b_1+2}+H_{n4}r^{b_1+1}
\end{aligned} \tag{38}$$

The Eq. (8) can be written in the rate form. Substituting Eq. (38) into rate form of Eq. (8), the complete solutions for displacement rates $\dot{u}(r,\theta)$ and $\dot{v}(r,\theta)$ are obtained as

$$\begin{aligned}
\dot{u}(r,\theta)&=\sum_{j=1}^{2}\left(C_{0j}+P_{0j}\right)r^{\gamma_{0j}}\\
&+\sum_{n=-\infty,n\neq 0}^{n=\infty}\left(\sum_{j=1}^{4}C_{nj}r^{\gamma_{nj}}+H_{n1}r^{b_1+2}+H_{n2}r^{b_1+1}\right)e^{in\theta}\\
\dot{v}(r,\theta)&=\sum_{j=3}^{4}\left(C_{0j}+P_{0j}\right)r^{\gamma_{0j}}\\
&+\sum_{n=-\infty,n\neq 0}^{n=\infty}\left(\sum_{j=1}^{4}N_{nj}C_{nj}r^{\gamma_{nj}}+H_{n3}r^{b_1+2}+H_{n4}r^{b_1+1}\right)e^{in\theta}
\end{aligned} \tag{39}$$

Substitution of Eq. (39) into rate form of Eq. (3) and using rate form of Eq. (8) for creep strains rates yields the stress rates as presented in Appendix B.

The initial elastic stress distribution at zero time may be obtained from the elastic solution.

4.4 Boundary conditions

Unknown constants C_{nj} (j = 1, 2, 3, 4) in displacement and stress relations can be obtained by applying four displacement and stress boundary conditions at inner and outer surfaces of FGM hollow cylinder. Furthermore two thermal boundary conditions are required for thermal unknown constants A_{nj} (j = 1, 2). Thus thermo-mechanical boundary conditions at the inner and outer radii are expressed as

$$\sigma_r(a,\theta) = 100\cos^2(\theta)\,\text{MPa} \qquad \sigma_{r\theta}(a,\theta) = 0$$

$$u(b,\theta) = 0 \qquad v(b,\theta) = 0 \tag{40}$$

$$T(a,\theta) = \left(500 + 50\cos(2\theta)\right)\,°C \qquad T(b,\theta) = 400\,°C$$

Substituting the first four boundary conditions of Eq. (40) into displacement and stress relations and using the Eqs. (24) and (25), the unknown coefficients C_{nj} (j = 1, 2, 3, 4) are calculated. Also using thermal boundary conditions and Eq. (A3) in Appendix A the unknown constants A_{nj} (j = 1, 2) are determined.

4.5 Numerical method

We have employed a numerical procedure to obtain histories of stresses, strains and displacements. Using the obtained stress rates from Section 4.3 we can calculate histories of stresses at any time t_i iteratively as Yang (2000).

$$\sigma_{ij}^{(i)}(t_i) = \sigma_{ij}^{(i-1)}(t_{i-1}) + \dot{\sigma}_{ij}^{(i-1)}(t_{i-1}).\Delta t^{(i)} \tag{41}$$

We need to point out that the initial elastic stresses at zero time will be redistributed due to creep. Having history of stresses from Eq. (41) one can determine strains and displacements histories using step by step procedure based on the flowchart presented in Fig. 2.

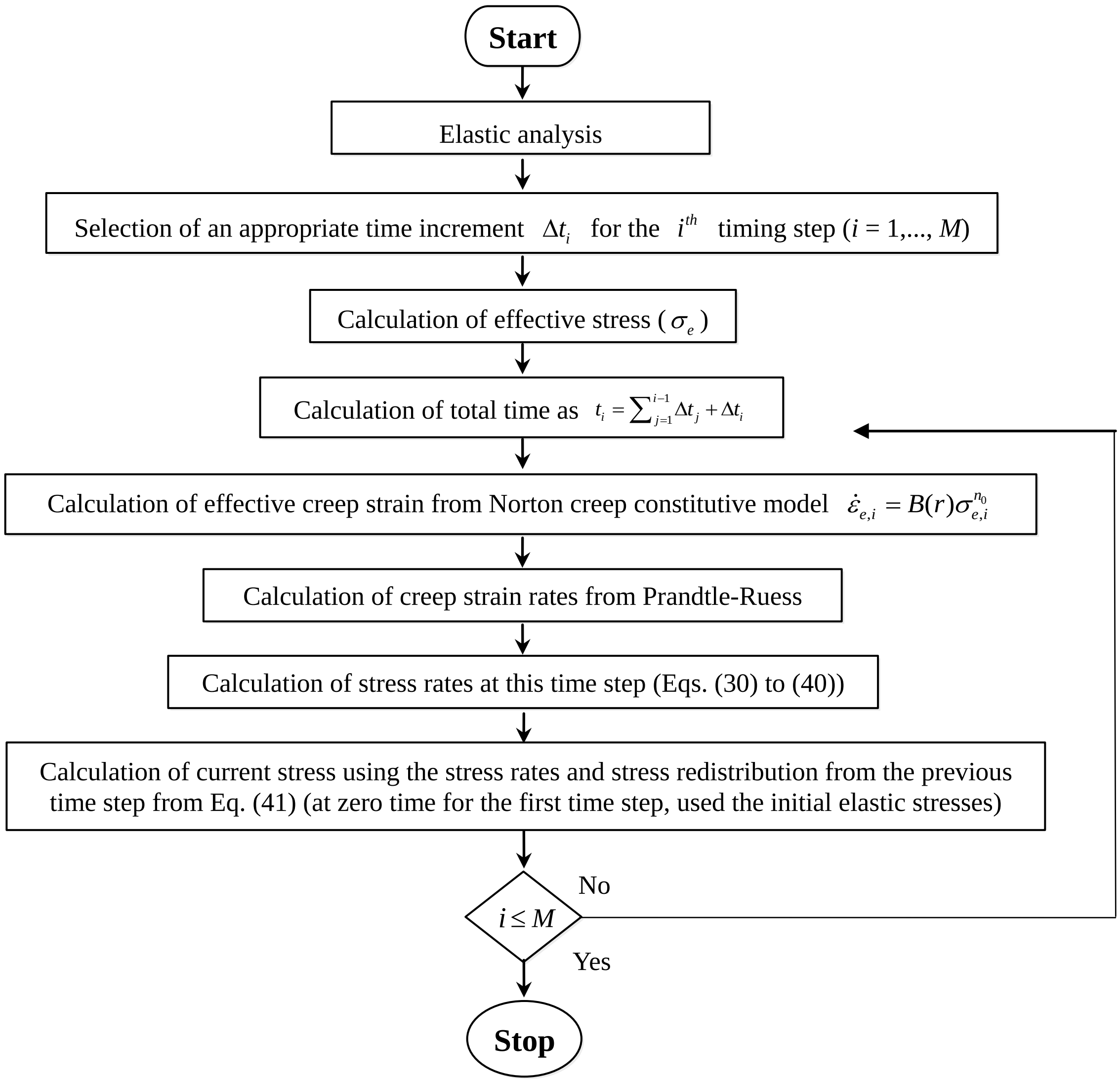

Fig. 2 Flowchart of time-dependent creep analysis of the cylinder

5. Results and discussion

5.1 Verification and validation

There are no results available in the literature for history of stresses and deformations of non-axisymmetric FGM cylinders. However with some simplification, our numerical results are compared with results presented by Loghman *et al*. (2010). The creep analysis of this problem was performed using the same method (Yang 2000) and the same creep constitutive model. Table 1 indicates comparison between the present results and Loghman *et al*. (2010) for similar material properties and boundary conditions at θ = 0. In another attempt, to validate the numerical results of the current problem, the results of creep analysis at zero time are compared with elastic solutions of the previous researches. For this purpose, the materials properties and boundary conditions are assumed in consistence with the existing literature. Figs. 3 and 4 illustrate temperature distribution and circumferential displacement of hollow FGM cylinder based on the data reported by Jabbari *et al*. (2003). The figures are identical to those reported in Figs. 1 and 3 of Jabbari *et al*. (2003) for the functionally graded hollow cylinder without any magnetic load ($\vec{H} = 0$).

5.2 Numerical results

The results presented in this paper are based on the following data of a thick-walled FGM cylinder (Xuan *et al*. 2009, Loghman *et al*. 2010).

Table 1 Comparison between present results and results of literature (Loghman *et al*. 2010 for the case β = +2 at θ = 0 after 3×10^8 seconds)

Dimensionless radius (r/b)	0.5	0.6	0.7	0.8	0.9	1
σ_r (Loghman *et al*. 2010)	-1	-0.9468	-0.7699	-0.5371	-0.2645	0
σ_r (Present study)	-1	-0.9465	-0.7697	-0.5368	-0.2641	0

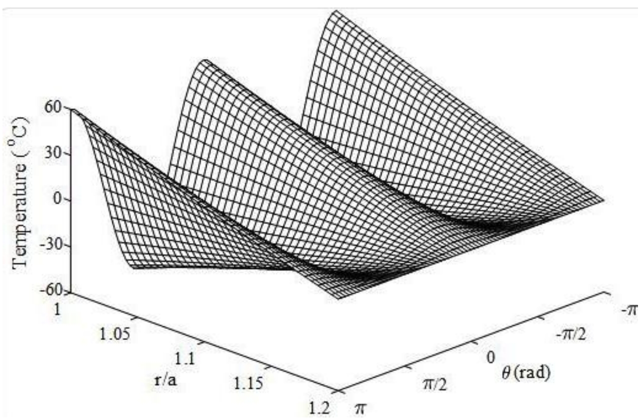

Fig. 3 Two dimensional non-symmetric temperature distribution of hollow FGM cylinder based on the data reported by Jabbari *et al*. (2003)

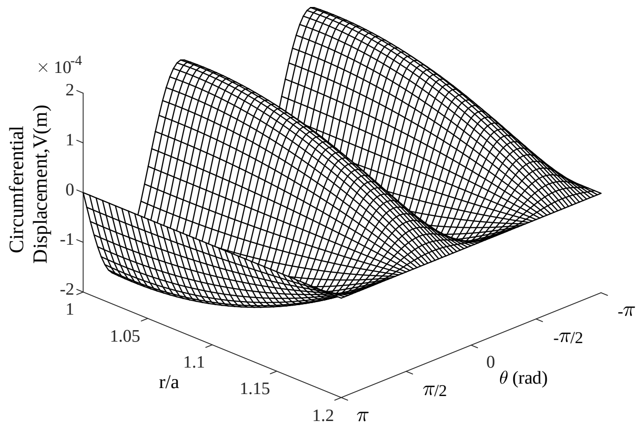

Fig. 4 Two dimensional non-symmetric distribution of circumferential displacement of hollow FGM cylinder based on the data reported by Jabbari *et al*. (2003)

$\alpha_i = 1.2\times10^{-6}\ 1/{}^\circ\mathrm{C}$, $H_z = 2.23\times10^{9}$ A/m ,

$\mu_i = 4\pi\times10^{-7}$ H/m , $E_i = 22$ GPa ,

$\upsilon = 0.3$, $b_0 = 0.11\times10^{-36}$, $b_1 = 5$,

$n_0 = 3$, $a/b = 0.5$

For simplicity of the analysis, power-law exponents of material properties have considered to be the same as $\beta_1 = \beta_2 = \beta_3 = \beta_4 = \beta$. Using boundary conditions and Eqs. (24)-(25) all terms except the terms associated with n = 0 and n = ±2 do not contribute to stresses and displacements distributions. According to the procedure of numerical analysis outlined in Section 4, all outputs including initial magneto-thermo-elastic responses and time-dependent creep stress, displacement redistributions and magnetic field component redistributions depicted in Figs. 5 to 16 are derived for functionally graded materials with β = 2. It is worth noting that dimensionless radial, circumferential and shear stresses are assumed as divide stress into absolute value of σ_r (a, 0) where it is 100 Mpa.

5.2.1 History of stresses and displacements

The two dimensional steady state temperature distribution in terms of dimensionless radius r/b and θ is illustrated in Fig. 5. As expected in applying the boundary conditions, the temperature at outer radius is constant and at inner radius of the cylinder changes based on the cosine functions. One can find that the maximum temperature is located at $\theta = 0 \pm \pi$.

Dimensionless radial, circumferential and shear stresses distributions versus dimensionless radius are demonstratedin Figs. 6-8, respectively. The obtained results indicate that the maximum radial, circumferential and shear stresses across the thickness direction are located at $\theta = \pm m\pi/4$ where m = 0, 4, m = 2 and m = 1, 3 respectively. It is observed that the circumferential and radial stresses along the circumferential direction at the outer surface are less than corresponding values at the inner surface. In addition, it is concluded that maximum variation of the shear stress is

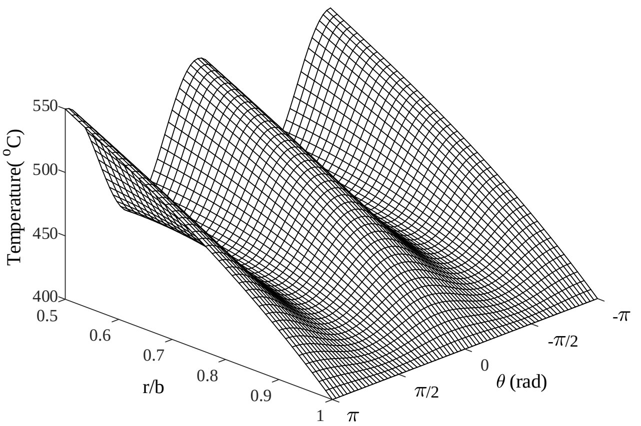

Fig. 5 Two dimensional non-symmetric distribution of temperature based on the thermal boundary condition considered in the present work

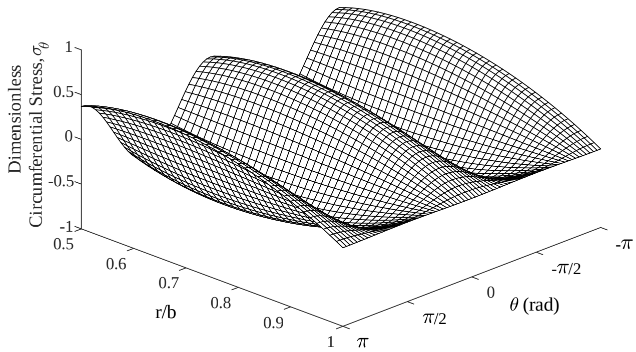

Fig. 7 Variation of initial circumferential stress of the FGM cylinder for the case $\beta = 2$

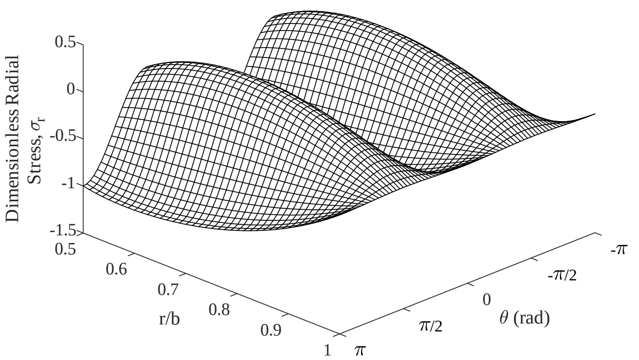

Fig. 6 Variation of initial radial stress of the FGM cylinder for the case $\beta = 2$

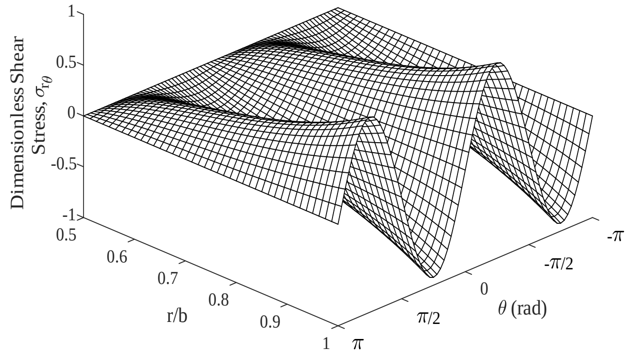

Fig. 8 Variation of initial shear stress of the FGM cylinder for the case $\beta = 2$

occurred at the outer surface and it is zero at the inner surface.

The redistribution of the radial stress at different creep times at $\theta = 0$ may be observed in Fig. 9(a). It is obvious from this figure that the radial stresses satisfy the boundary condition at the inner radii and are not zero at the outer surface due to zero displacement boundary condition at the outer radii. The numerical results show that maximum radial stress is occurred at location $r/b = 0.58$ for zero time. This point moves to inner surface after 50 years of creep. Furthermore, we can conclude that the absolute values of

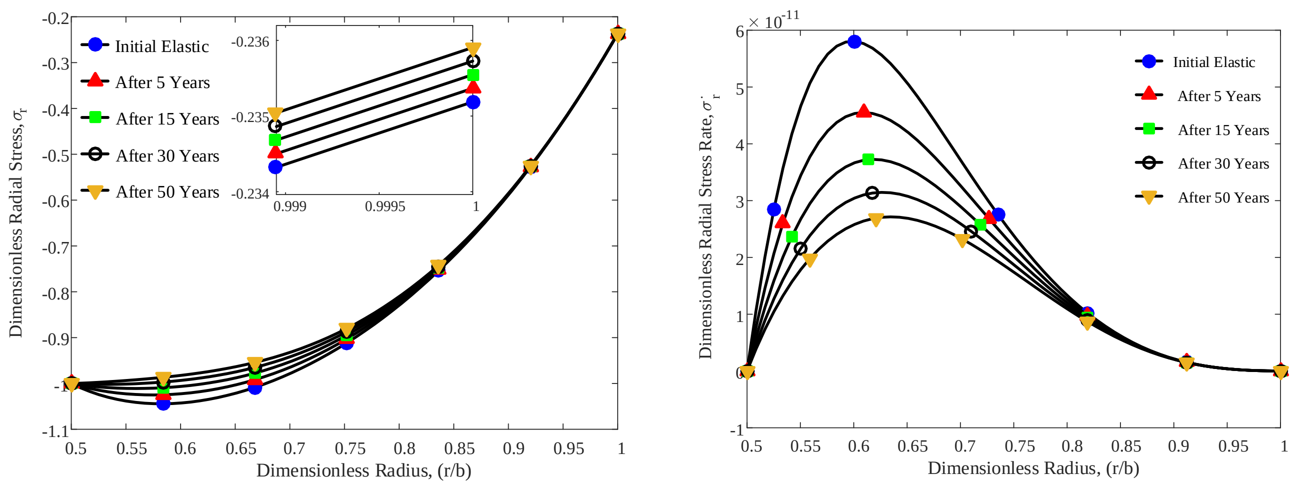

(a) Radial stress redistribution

(b) The rate of radial stress redistribution

Fig. 9 Radial creep stress and the rate of it for the FGM cylinder at $\theta = 0$ from initial case up to 50 years for the case $\beta = 2$

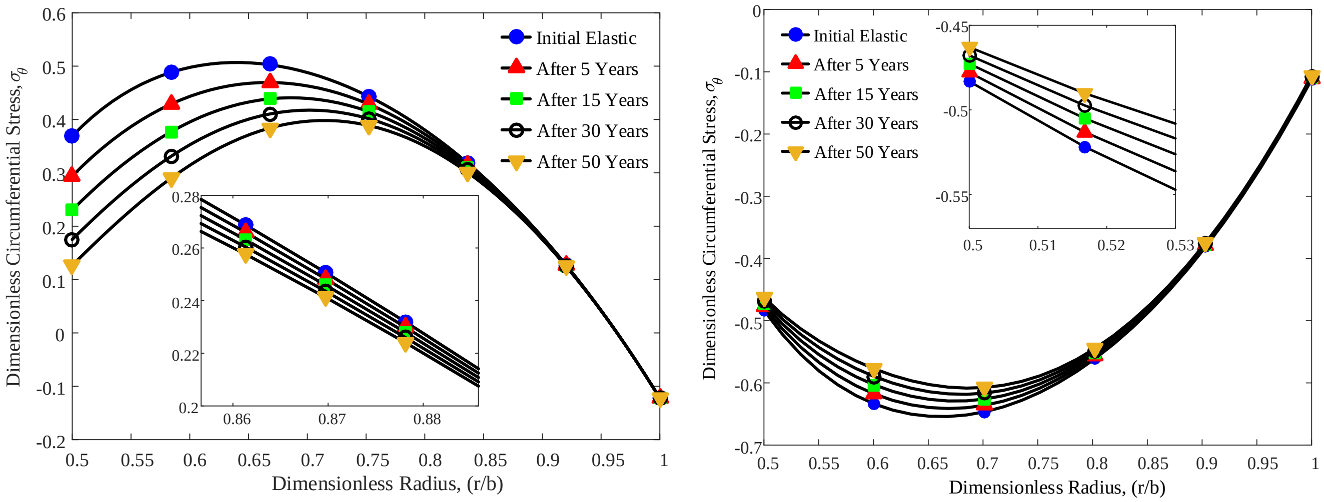

(a) $\theta = 0$ (b) $\theta = \pi/2$

Fig. 10 The redistribution of circumferential creep stress of FGM cylinder at $\theta = 0$ and $\theta = \pi/2$ from initial elastic case up to 50 years for the case

Table 2 The values of dimensionless radial, circumferential and shear stresses at different angles after 50 years

Dimensionless stress	Angle	Dimensionless radius (r/b)					
		0.5	0.6	0.7	0.8	0.9	1
σ_r	0	-1	-0.9831	-0.9325	-0.8088	-0.5796	-0.2249
	30	-0.75	-0.7014	-0.6397	-0.5472	-0.4119	-0.2236
	45	-0.5	-0.3954	-0.3284	-0.2823	-0.2486	-0.2232
	60	-0.25	-0.0759	-0.0094	-0.0151	-0.0858	-0.2235
	90	0	0.2337	0.3027	0.2531	0.0812	-0.2247
σ_θ	0	0.1324	0.321	0.4050	0.3587	0.1826	-0.1171
	30	0.0776	0.1655	0.1804	0.1347	0.0345	-0.1188
	45	-0.0676	-0.0735	-0.0836	-0.0985	-0.1069	-0.1194
	60	-0.2741	-0.3516	-0.3627	-0.3280	-0.2479	-0.1188
	90	-0.4767	-0.6016	-0.6281	-0.5628	-0.3948	-0.1170
$\sigma_{r\theta}$	0	0	0	0	0	0	0
	30	0	-0.0805	-0.1417	-0.2358	-0.3603	-0.5018
	45	0	-0.1403	-0.2139	-0.2952	-0.3978	-0.5278
	60	0	-0.1311	-0.1902	-0.2698	-0.3749	-0.5018
	90	0	0	0	0	0	0

Furthermore, we can conclude that the absolute values of radial stress are decreased with increase of creep time and finally reach to steady state condition. The rate of time-dependent creep radial stress at $\theta = 0$ is illustrated in Fig. 9(b). It is concluded that this rate is decreased with increase of creep time and is arrived to steady state condition for long interval of creep times.

The redistribution of circumferential stress at different creep times are plotted in Figs. 10(a) and (b) at $\theta = 0$ and $\theta = \pi/2$, respectively. This figure indicates that the value of circumferential stresses is decreased with increase of creep time. It is concluded that for the case $\theta = \pi/2$ the location of maximum circumferential stress is moved to outer surface while for $\theta = 0$, it is moved toward inner surface as the time is increased. It could be argued that the results due to non-axisymmetric loading are not same for different angles.

Time dependent creep shear stress redistributions at $\theta = \pi/4$ for the case $\beta = 2$ is presented in Fig. 11. The obtained results in this figure indicate that the absolute value of shear stress is decreased with increase of creep time. For comparison, the numerical values of radial, circumferential and shear stresses after 50 years at different angular positions are presented in Table 2.

History of radial and circumferential displacements versus dimensionless radius is plotted in Figs. 12 and 13 respectively. The boundary conditions are satisfied at the

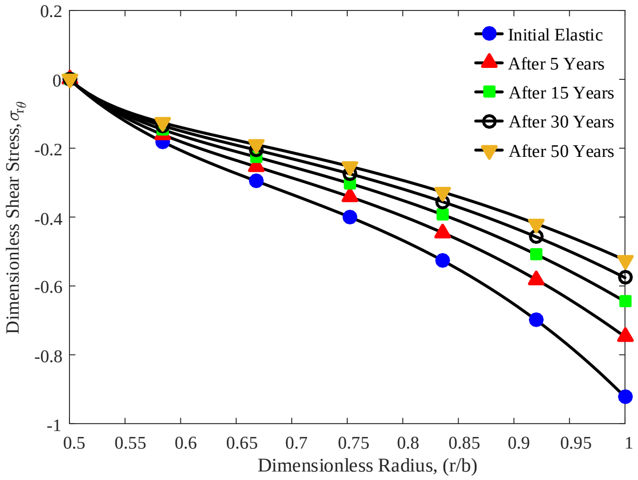

Fig. 11 Redistribution of creep shear stress of the FGM cylinder at $\theta = \pi/4$ from initial elastic up to 50 years for the case

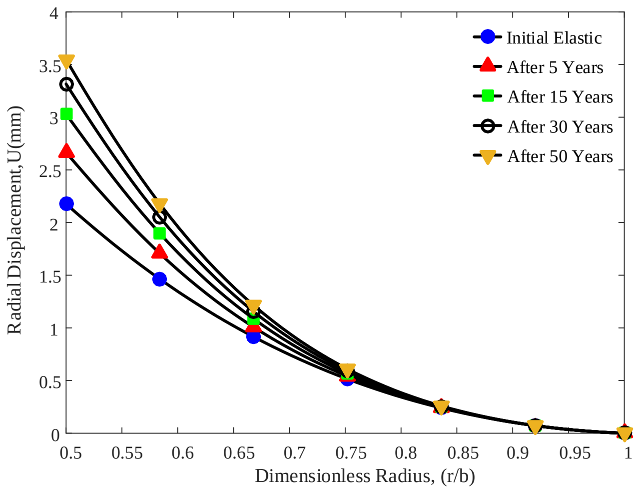

Fig. 12 Redistribution of radial displacement of the FGM cylinder at $\theta = 0$ from initial elastic case up to 50 years for the case $\beta = 2$

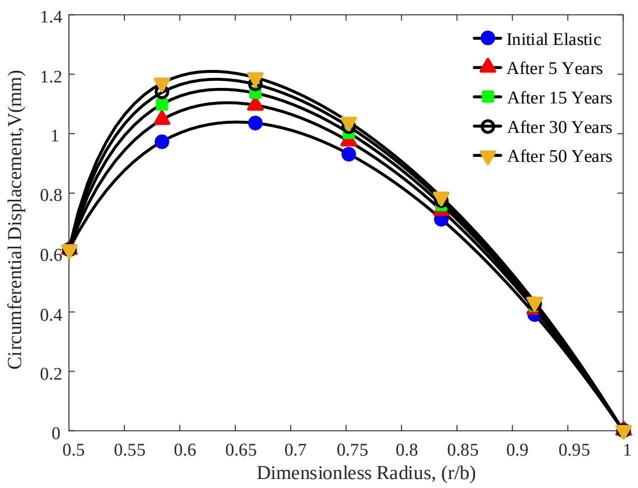

Fig. 13 Redistribution of circumferential displacement of the FGM cylinder at $\theta = \pi/4$ from initial elastic case up to 50 years for the case $\beta = 2$

exterior surface of the FGM cylinder in two figures. The maximum values of radial displacements are occurred at the inner surface while circumferential displacement has a maximum value located almost at one third portion of the thickness near to inner surface.

5.2.2 History of magnetic field components

Based on Eq. (5), Lorent'z force, perturbation of magnetic field vector and perturbation of electric field vector are depending on the radial and circumferential displacements. Fig. 14 demonstrates the history of radial Lorent'z force at $\theta = 0$ from initial elastic solution up to 50 years. As it can be seen, the radial Lorent'z force is increased with increase of creep time.

Initial magnetothermoelastic circumferential Lorent'z force at zero time are showed in Fig. 15. Our numericalresults indicate that circumferential Lorent'z force is approximately stationary with time and is assumed equal to elastic case. The axial perturbation of magnetic field, h_z, is depicted in Fig. 16(a). As can be seen in this figure the maximum h_z at $\theta = 0$, π and $\theta = \pm\pi/2$ are equal in magnitude but opposite in sign. In addition, the history of h_z at $\theta = 0$ is

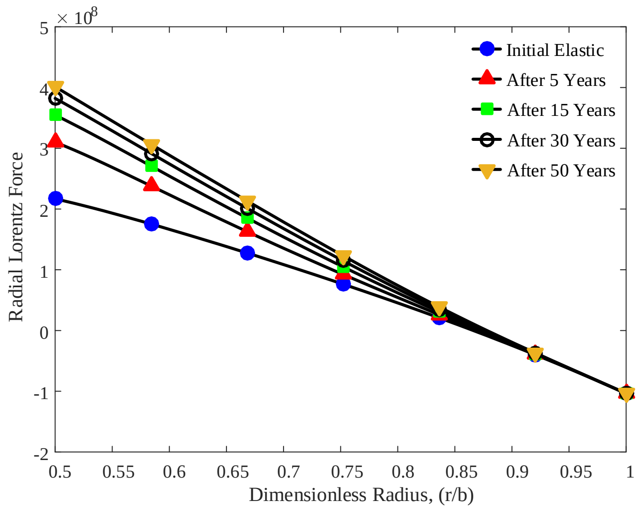

Fig. 14 Redistribution of radial Lorentz force of FGM cylinder at $\theta = 0$ from initial elastic case up to 50 years for the case $\beta = 2$

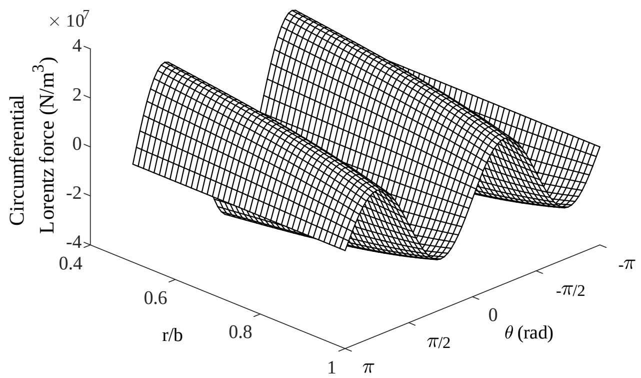

Fig. 15 Distribution of circumferential Lorentz force of FGM cylinder at zero time for the case $\beta = 2$

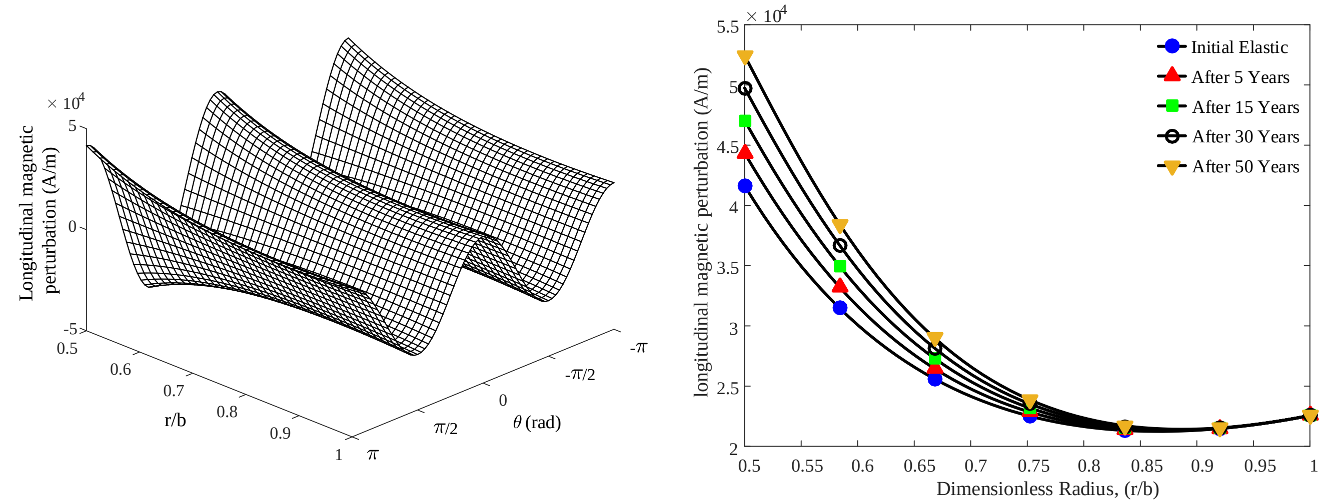

(a) Distribution of longitudinal magnetic perturbation at zero time (b) Redistribution of longitudinal magnetic perturbation at $\theta = 0$

Fig. 16 Distribution and redistribution of longitudinal magnetic perturbation of the FGM cylinder for the case $\beta = 2$

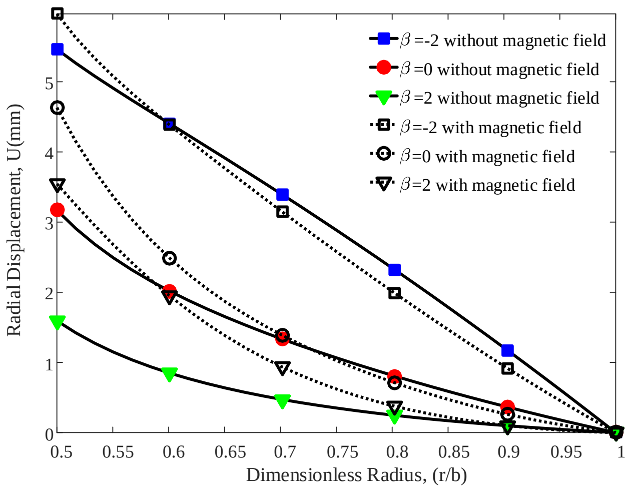

Fig. 17 Effect of material inhomogeneity index and magnetic field on radial displacement of the cylinder at $\theta = 0$ after 50 years

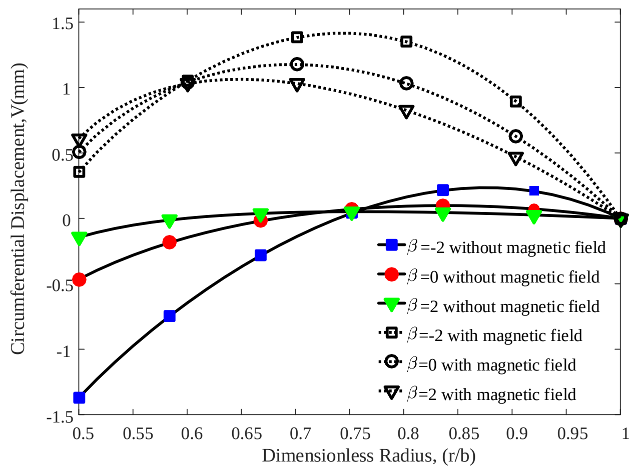

Fig. 18 Effect of material inhomogeneity index and magnetic field on circumferential displacement of the cylinder at $\theta = \pi/4$ after 50years

presented in Fig. 16(b). This figures indicates that changes of this parameter at inner radius is very significant rather than one at outer radius due to imposing the inner boundary conditions.

5.2.3 Effect of material inhomogeneity index and magnetic field

The effect of in-homogeneity parameter, β, and magnetic field on displacements and stresses along the radius of cylinder after 50 years are studied in Figs. 17-21. From Fig. 17, one can conclude that increase of in-homogeneity index leads to decrease of radial displacement throughout thickness for two cases of with and without magnetic field. This decrease is due to increase of stiffness of material that prevents the further displacement. Also the presence of magnetic field almost increases the amount of radial displacement.

Shown in Fig. 18 is the circumferential displacement of cylinder for various values of in-homogeneity index with and without magnetic field. As can be seen, existence of magnetic field leads to basically changes of the behavior of curves. In addition, the behavior of circumferential displacement due to change of in-homogeneity index is strongly depending on the radial location. However these results confirm that the maximum and minimum values of circumferential displacement belong to $\beta = -2$ and $\beta = 2$ respectively.

Figs. 19-21 show the influence of in-homogeneity index and magnetic field on the radial, circumferential and shear stresses after 50 years. It can be concluded that for $\beta = -2$, employing the magnetic field leads to lower radial stress while for $\beta = 0$ and $\beta = 2$ radial stress decreases in the 0.74-1 and 0.91-1 range of r/b respectively. In general, radial stress is decreased at outer surface with existence of magnetic field. In addition, it is observed that increase of in-homogeneity index significantly increases the radial stress.

To clarify the effect of magnetic field and β at various angles, the distribution of circumferential stress is plotted at $\theta = 0$ and $\theta = \pi/2$ in Fig. 20. The change of magnetic field,

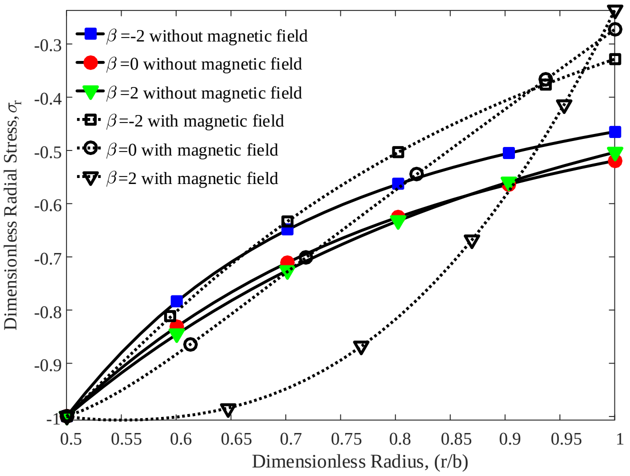

Fig. 19 Effect of material inhomogeneity index and magnetic field on dimensionless radial stress of the cylinder at $\theta = 0$ after 50 years

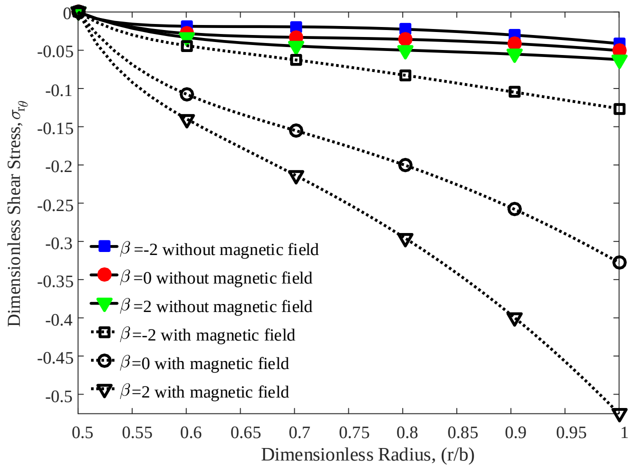

Fig. 21 Effect of material inhomogeneity index and magnetic field on shear stress of the cylinder at $\pi/4$ after 50 years

in-homogeneous index and radial location leads to significant and interesting change of responses as depicted in Figs. 20(a) and (b). It is observed that the behavior of circumferential stress for $\beta = 2$ is basically differs from one for $\beta = 0, -2$. It is concluded that the circumferential stress for $\beta = 2$ has a maximum value at middle of the wall of cylinder while for $\beta = 0, -2$ the circumferential stress is decreased along the thickness direction. In addition, addition of magnetic field leads to significant increase of circumferential stress.

Fig. 21 indicates that in presence of magnetic field, the absolute value of shear stress is increased significantly. The minimum and maximum of shear stress in the FGM vessel belong to $\beta = -2$ and $\beta = -2$ respectively.

6. Conclusions

Time-dependent magnetothermoelastic creep stress redistribution analysis of a functionally graded cylindrical vessel subjected to non-axisymmetric thermo-mechanical and uniform magnetic loadings was studied in this paper. Two governing differential equations of system were derived based on two dimensional non-axisymmetric displacement field with considering thermal effects. The important results of the present paper may be classified as follows:

(1) It was concluded that the maximum values of radial, circumferential and shear stresses through-thickness are located at $\theta = \pm m\pi/4$ where $m = 0, 4$, $m = 2$ and $m = 1, 3$ respectively.
(2) As a main conclusion based on the obtained results of Figs. 9-11, we can conclude that the absolute values of radial, circumferential and shear stresses are decreased with increase of creep time and finally reach to steady state condition.
(3) Both radial and circumferential displacements are

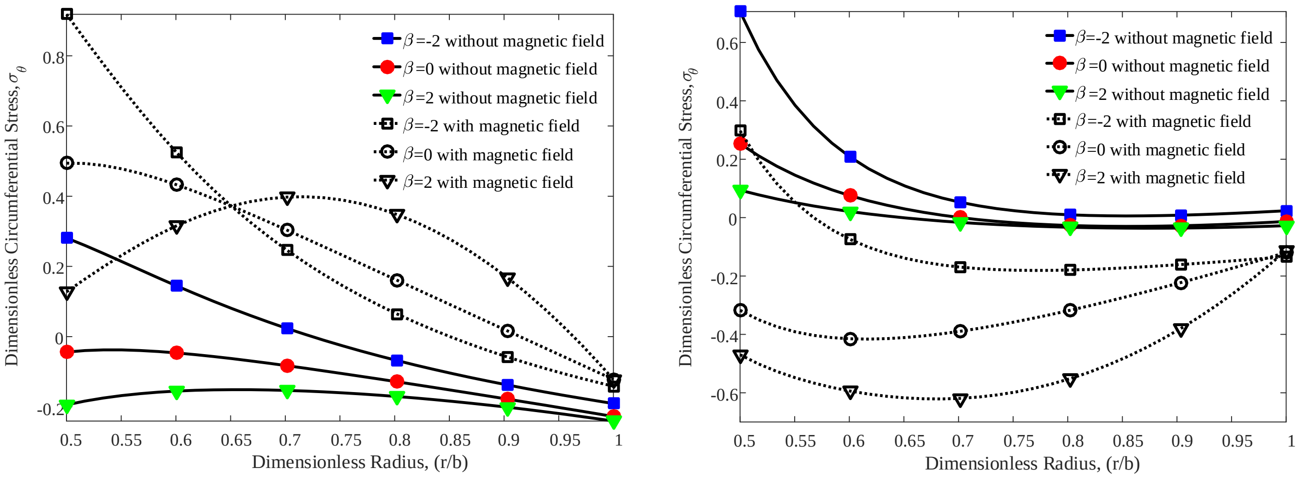

(a) $\theta = 0$ (b) $\theta = \pi/2$

Fig. 20 Effect of material inhomogeneity index and magnetic field on dimensionless circumferential stress in the FGM cylinder at $\theta = 0$ and $\theta = \pi/2$ after 50 years increased with increase of creep during so that they finally approach to steady state condition. Also the lower values of radial and circumferential displacements are occurred for $\beta = 2$.

(4) It was found that with existence of magnetic field and increasing the material inhomogeneity index, the radial displacement is decreased across the cylinder thickness; however, the behavior of circumferential displacement, radial and circumferential stresses are strongly depending on the material in-homogeneity index.

Acknowledgments

The research described in this paper was financially supported by the University of Kashan.

References

Arani, A.G., Barzoki, A.M., Kolahchi, R., Mozdianfard, M.R. and Loghman, A. (2011), "Semi-analytical solution of time-dependent electro-thermo-mechanical creep for radially polarized piezoelectric cylinder", *Comput. Struct.*, **89**(15), 1494-502.

Arani, A.G., Haghparast, E., Maraghi, Z.K. and Amir, S. (2015), "Static stress analysis of carbon nano-tube reinforced composite (CNTRC) cylinder under non-axisymmetric thermo-mechanical loads and uniform electro-magnetic fields", *Compos. Part B. Eng.*, **68**, 136-145.

Arefi, M. (2014), "A complete set of equations for piezo-magnetoelastic analysis of a functionally graded thick shell of revolution", *Latin. Am. J. Solids. Struct.*, **11**(11), 2073-2092.

Arefi, M. (2015), "Nonlinear electromechanical analysis of a functionally graded square plate integrated with smart layers resting on Winkler-Pasternak foundation", *Smart. Struct. Syst., Int. J.*, **16**(1), 195-211.

Arefi, M. (2016a), "Analysis of wave in a functionally graded magneto-electro-elastic nano-rod using nonlocal elasticity model subjected to electric and magnetic potentials", *Acta Mech.*, **227**(9), 2529-2542.

Arefi, M. (2016b), "Surface effect and non-local elasticity in wave propagation of functionally graded piezoelectric nano-rod excited to applied voltage", *Appl. Math. Mech.*, **37**(3), 289-302.

Arefi, M. and Allam, M.N.M. (2015), "Nonlinear responses of an arbitrary FGP circular plate resting on foundation", *Smart Struct. Syst., Int. J.*, **16**(1), 81-100.

Arefi, M. and Nahas, I. (2014), "Nonlinear electro thermo elastic analysis of a thick spherical functionally graded piezoelectric shell", *Compos. Struct.*, **118**, 510-518.

Arefi, M. and Rahimi, G.H. (2011a), "Thermo elastic analysis of a functionally graded cylinder under internal pressure using first order shear deformation theory", *Sci. Res. Essays.*, **5**(12), 1442-454.

Arefi, M. and Rahimi, G.H. (2011b), "Nonlinear analysis of a functionally graded square plate with two smart layers as sensor and actuator under normal pressure", *Smart. Struct. Syst., Int. J.*, **8**(5), 433-447.

Arefi, M. and Rahimi, G.H. (2012a), "The effect of nonhomogeneity and end supports on the thermo elastic behavior of a clamped-clamped FG cylinder under mechanical and thermal loads", *Int. J. Pres. Ves. Pip.*, **96**, 30-37.

Arefi, M. and Rahimi, G.H. (2012b), "Comprehensive thermoelastic analysis of a functionally graded cylinder with different boundary conditions under internal pressure using first order shear deformation theory", *Mechanika*, **18**(1), 5-13.

Arefi, M. and Rahimi, G.H. (2012c), "Studying the nonlinear behavior of the functionally graded annular plates with piezoelectric layers as a sensor and actuator under normal pressure", *Smart. Struct. Syst., Int. J.*, **9**(2), 127-143.

Arefi, M. and Rahimi, G.H. (2012d), "Three-dimensional multi-field equations of a functionally graded piezoelectric thick shell with variable thickness, curvature and arbitrary nonhomogeneity", *Acta. Mech.*, **223**(1), 63-79.

Arefi, M. and Rahimi, G.H. (2014a), "Application of shear deformation theory for two dimensional electro-elastic analysis of a FGP cylinder", *Smart. Struct. Syst., Int. J.*, **13**(1), 1-24.

Arefi, M. and Rahimi, G.H. (2014b), "Comprehensive piezo-thermo-elastic analysis of a thick hollow spherical shell", *Smart. Struct. Syst., Int. J.*, **14**(2), 225-246.

Arefi, M. and Zenkour, A.M. (2016a), "Free vibration, wave propagation and tension analyses of a sandwich micro/nano rod subjected to electric potential using strain gradient theory", *Mater. Res. Exp.*, **3**(11), 115704.

Arefi, M. and Zenkour, A.M. (2017b), "Transient sinusoidal shear deformation formulation of a size-dependent three-layer piezo-magnetic curved nanobeam", *Acta. Mech.*, **228**(10) 3657-3674.

Arefi, M. and Zenkour, A.M. (2017a), "Influence of magneto-electric environments on size-dependent bending results of three-layer piezomagnetic curved nanobeam based on sinusoidal shear deformation theory", *J. Sandw. Struct. Mater.* [In Press]

Arefi, M. and Zenkour, A.M. (2017b), "Nonlocal electro-thermo-mechanical analysis of a sandwich nanoplate containing a Kelvin–Voigt viscoelastic nanoplate and two piezoelectric layers", *Acta. Mech.*, **228**(2), 475-493.

Arefi, M. and Zenkour, A.M. (2017c), "Thermo-electro-mechanical bending behavior of sandwich nanoplate integrated with piezoelectric face-sheets based on trigonometric plate theory", *Compos. Struct.*, **162**, 108-122.

Arefi, M. and Zenkour, A.M. (2017d), "Size-dependent vibration and bending analyses of the piezomagnetic three-layer nanobeams", *Appl. Phys. A.*, **123**(3), 202.

Arefi, M. and Zenkour, A.M. (2017e), "Wave propagation analysis of a functionally graded magneto-electro-elastic nanobeam rest on Visco-Pasternak foundation", *Mech. Res. Com.*, **79**, 51-62.

Arefi, M. and Zenkour, A.M. (2017f), "Effect of thermo-magneto-electro-mechanical fields on the bending behaviors of a three-layered nanoplate based on sinusoidal shear-deformation plate theory", *J. Sandw. Struct. Mater.*, 1099636217697497.

Arefi, M. and Zenkour, A.M. (2017g), "Employing the coupled stress components and surface elasticity for nonlocal solution of wave propagation of a functionally graded piezoelectric Love nanorod model", *J. Intel. Mater. Syst. Struct.*, **28**(17), 2403-2413.

Arefi, M. and Zenkour, A.M. (2017h), "Employing sinusoidal shear deformation plate theory for transient analysis of three layers sandwich nanoplate integrated with piezo-magnetic face-sheets", *Smart. Mater. Struct.*, **25**(11), 115040.

Arefi, M. and Zenkour, A.M. (2017i), "Vibration and bending analysis of a sandwich microbeam with two integrated piezo-magnetic face-sheets", *Compos. Struct.*, **159**(1), 479-490.

Arefi, M., Rahimi, G.H. and Khoshgoftar, M.J. (2011), "Optimized design of a cylinder under mechanical, magnetic and thermal loads as a sensor or actuator using a functionally graded piezomagnetic material", *Int. J. Phys. Sci.*, **6**(27), 6315-6322.

Arefi, M., Rahimi, G.H. and Khoshgoftar, M.J. (2012), "Exact solution of a thick walled functionally graded piezoelectric cylinder under mechanical, thermal and electrical loads in the magnetic field", *Smart. Struct. Syst., Int. J.*, **9**(5), 427-439.

Arefi, M., Zamani, M.H. and Kiani, M. (2017), "Size-dependent free vibration analysis of three-layered exponentially graded nanoplate with piezomagnetic face-sheets resting on Pasternak's foundation", *J. Intel. Mater. Syst. Struct.*, **29**(5), 774-786.

Boyce, W.E., DiPrima, R.C. and Haines, C.W. (1969), *Elementary Differential Equations and Boundary Value Problems*, Wiley, New York, USA.

Brnic, J., Canadija, M., Turkalj, G., Krscanski, S., Lanc, D., Brcic, M. and Gao, Z. (2016), "Short-time creep, fatigue and mechanical properties of 42CrMo4 - Low alloy structural steel", *Steel Compos. Struct., Int. J.*, **22**(4), 875-888.

Fesharaki, J.J. Fesharaki, V.J., Yazdipoor, M. and Razavian, B. (2012), "Two-dimensional solution for electro-mechanical behavior of functionally graded piezoelectric hollow cylinder", *Appl. Math. Model.*, **36**(11), 5521-5533.

Firouz-Abadi, R.D., Hojjati, M. and Rahmanian, M. (2014), "Free vibrations of single walled carbon peapods", *Physica E.*, **56**, 410-413.

Gallo, P., Berto, F. and Glinka, G. (2016), "Analysis of creep stresses and strains around sharp and blunt V-notches", *Theor. Appl. Fract. Mech.*, **85**, 435-446.

Ginder, R.S., Nix, W.D. and Pharr, G.M. (2018), "A simple model for indentation creep", *J. Mech. Physics of Solids.*, **112**, 552-562.

Golmakaniyoon, S. and Akhlaghi, F. (2016), "Time-dependent creep behavior of Al--SiC functionally graded beams under in-plane thermal loading", *Comput. Mat. Sci.*, **121**, 182-190.

Hetnarski, R.B., Eslami, M.R. and Gladwell, G.M.L. (2009), *Thermal Sresses-Avanced Theory and Applications*, Springer, Dordrecht, Netherlands.

Jabbari, M., Sohrabpour, S. and Eslami, M.R. (2003), "General solution for mechanical and thermal stresses in a functionally graded hollow cylinder due to nonaxisymmetric steady-state loads", *J. Appl. Mech.*, **70**(1), 111-118.

Jabbari, M., Vaghari, A.R., Bahtui, A. and Eslami, M.R. (2008), "Exact solution for asymmetric transient thermal and mechanical stresses in FGM hollow cylinders with heat source", *Struct. Eng. Mech., Int. J.*, **29**(5), 551-565.

Jain, P.K. and Singh, S. (2009), "Analytical solution to transient asymmetric heat conduction in a multilayer annulus", *J. Heat Trans., ASME*, **131**(1), 11304.

Lee, K.H. and Fenner, R.T. (1986), "A quadratic formulation for two-dimensional elastoplastic analysis using the boundary integral equation method", *J. Strain. Analysis. Eng. Des.*, **21**(3), 159-175.

Li, H. and Liu, Y. (2014), "Functionally graded hollow cylinders with arbitrary varying material properties under nonaxisymmetric loads", *Mech. Res. Commun.*, **55**, 1-9.

Loghman, A. and Wahab, M.A. (1996), "Creep damage simulation of thick-walled tubes using the θ projection concept", *Int. J. Pres. Ves. Pip.*, **67**(1), 105-111.

Loghman, A., Arani, A.G, Amir, S. and Vajedi, A. (2010), "Magnetothermoelastic creep analysis of functionally graded cylinders", *Int. J. Pres. Ves. Pip.*, **87**(7), 389-395.

Loghman, A., Abdollahian, M., Jazi, A.J. and Arani, A.G. (2013), "Semi-analytical solution for electromagnetothermoelastic creep response of functionally graded piezoelectric rotating disk", *Int. J. Thermal. Sci.*, **65**, 254-266.

Loghman, A., Nasr, M. and Arefi, M. (2017), "Nonsymmetric thermomechanical analysis of a functionally graded cylinder subjected to mechanical, thermal, and magnetic loads", *J. Therm. Stress.*, **40**(6), 765-782.

Loghman, A., Faegh, R.K. and Arefi, M. (2018), "Two dimensional time-dependent creep analysis of a thick-walled FG cylinder based on first order shear deformation theory", *Steel Compos. Struct., Int. J.*, **26**(5), 533-547.

Mangal, S.K., Kapoor, N. and Singh, T. (2013), "Steady-State Creep Analysis of Functionally Graded Rotating Cylinder", *Strain.*, **49**(6), 457-466.

Mendelson, A. (1968), *Plasticity Theory and Application*, Macmillan, New York, NY, USA.

Nejad, M.Z. and Kashkoli, M.D. (2014), "Time-dependent thermo-creep analysis of rotating FGM thick-walled cylindrical pressure vessels under heat flux", *Int. J. Engineer Sci.*, **82**, 222-237.

Ootao, Y. and Ishihara, M. (2013), "Asymmetric transient thermal stress of a functionally graded hollow cylinder with piecewise power law", *Struct. Eng. Mech., Int. J.*, **47**(3), 421-442.

Penney, R.K. and Marriott, D.L. (1971), *Design for Creep*, McGraw-Hill, London, UK.

Poultangari, R., Jabbari, M. and Eslami, M.R. (2008), "Functionally graded hollow spheres under non-axisymmetric thermo-mechanical loads", *Int. J. Pres. Ves. Pip.*, **85**(5), 295-305.

Rahimi, G.H., Arefi, M. and Khoshgoftar, M.J. (2012), "Electro elastic analysis of a pressurized thick-walled functionally graded piezoelectric cylinder using the first order shear eformation theory and energy method", *Mechanika*, **18**(3), 292-300.

Rice, R.G. and Do, D.D. (2012), *Applied Mathematics and Modeling for Chemical Engineers*, John Wiley & Sons, NJ, USA.

Sadd, M.H. (2009), *Elasticity*: *Theory, Applications and Numerics*, Academic Press, Burlington, NJ, USA.

Sahan, M.F. (2015), "Transient analysis of cross-ply laminated shells using FSDT: Alternative formulation", *Steel Compos. Struct., Int. J.*, **18**(4), 889-907.

Shao, Z.S., Ang, K.K., Reddy, J.N. and Wang, T.J. (2008), "Nonaxisymmetric thermomechanical analysis of functionally graded hollow cylinders", *J. Therm. Stress.*, **31**(6), 515-536.

Xuan, F.Z., Chen, J.J., Wang, Z. and Tu, S.T. (2009), "Time-dependent deformation and fracture of multi-material systems at high temperature", *Int. J. Pres. Ves. Pip.*, **86**(9), 604-615.

Yang, Y.Y. (2000), "Time-dependent stress analysis in functionally graded materials", *Int. J. Solids. Struct.*, **37**(51), 7593-7608.

You, L.H., Ou, H. and Zheng, Z.Y. (2007), "Creep deformations and stresses in thick-walled cylindrical vessels of functionally graded materials subjected to internal pressure", *Compos. Struct.*, **78**(2), 285-291.

Zenkour, A.M. and Arefi, M. (2017), "Nonlocal transient electrothermomechanical vibration and bending analysis of a functionally graded piezoelectric single-layered nanosheet rest on visco-Pasternak foundation", *J. Therm. Stress.*, **40**(2), 167-184.

CC

Appendix A

The constants in Eq. (7) are written as

$$
\begin{array}{llll}
s_1 = 1+\beta_1 I & s_2 = \dfrac{\upsilon\beta_1}{1-\upsilon}I-1 & s_3 = \dfrac{1-2\upsilon}{2-2\upsilon}I & s_4 = 1-I+\dfrac{I}{2-2\upsilon} \\
\multicolumn{2}{l}{s_5 = -1+I\left(1+\dfrac{(4+2\beta_1)\upsilon-3}{2-2\upsilon}\right)} & \multicolumn{2}{l}{s_6 = \dfrac{1+\upsilon}{1-\upsilon}\alpha_i(\beta_1+\beta_2)I} \\
s_7 = \dfrac{1+\upsilon}{1-\upsilon}\alpha_i I & s_8 = s_1+2s_3-1 & s_9 = s_4+s_5 & s_{10} = I \\
s_{11} = \dfrac{\upsilon}{1-\upsilon}I & s_{12} = 2s_3 & s_{13} = 1+\beta_1 & s_{14} = -s_{13} \\
s_{15} = J+\dfrac{2-2\upsilon}{1-2\upsilon} & s_{16} = J+\dfrac{1}{1-2\upsilon} & s_{17} = J+\dfrac{3-4\upsilon}{1-2\upsilon}+\beta_1 & s_{18} = \dfrac{2+2\upsilon}{1-2\upsilon}\alpha_i \\
s_{19} = 2\beta_1+4 & s_{20} = 2 & s_{21} = \dfrac{2\upsilon}{1-2\upsilon} & s_{22} = \dfrac{2-2\upsilon}{1-2\upsilon}
\end{array}
\tag{A1}
$$

Where

$$
I = \frac{E_i(1-\upsilon)}{\mu_i H_z^2(1+\upsilon)(1-2\upsilon)+E_i(1-\upsilon)} \qquad J = \frac{2\mu_i H_z^2(1+\upsilon)}{E_i} \tag{A2}
$$

The unknown constants in Eq. (11) are

$$
\begin{aligned}
A_{n1} &= \frac{\dfrac{1}{2\pi}\displaystyle\int_{-\pi}^{\pi}\left[\left(\chi_{21}b^{\zeta_{n2}}+\chi_{22}\zeta_{n2}b^{\zeta_{n2}-1}\right)F_1(\theta)-\left(\chi_{11}a^{\zeta_{n2}}+\chi_{12}\zeta_{n2}a^{\zeta_{n2}-1}\right)F_2(\theta)\right]e^{-in\theta}d\theta}{\left(\chi_{11}a^{\zeta_{n1}}+\chi_{12}\zeta_{n1}a^{\zeta_{n1}-1}\right)\left(\chi_{21}b^{\zeta_{n2}}+\chi_{22}\zeta_{n2}b^{\zeta_{n2}-1}\right)-\left(\chi_{11}a^{\zeta_{n2}}+\chi_{12}\zeta_{n2}a^{\zeta_{n2}-1}\right)\left(\chi_{21}b^{\zeta_{n1}}+\chi_{22}\zeta_{n1}b^{\zeta_{n1}-1}\right)} \\
A_{n2} &= \frac{\dfrac{1}{2\pi}\displaystyle\int_{-\pi}^{\pi}\left[\left(\chi_{11}a^{\zeta_{n1}}+\chi_{12}\zeta_{n1}a^{\zeta_{n1}-1}\right)F_2(\theta)-\left(\chi_{21}b^{\zeta_{n1}}+\chi_{22}\zeta_{n1}b^{\zeta_{n1}-1}\right)F_1(\theta)\right]e^{-in\theta}d\theta}{\left(\chi_{11}a^{\zeta_{n1}}+\chi_{12}\zeta_{n1}a^{\zeta_{n1}-1}\right)\left(\chi_{21}b^{\zeta_{n2}}+\chi_{22}\zeta_{n2}b^{\zeta_{n2}-1}\right)-\left(\chi_{11}a^{\zeta_{n2}}+\chi_{12}\zeta_{n2}a^{\zeta_{n2}-1}\right)\left(\chi_{21}b^{\zeta_{n1}}+\chi_{22}\zeta_{n1}b^{\zeta_{n1}-1}\right)}
\end{aligned}
\tag{A3}
$$

The constants and powers in Eq. (18) are

$$
\begin{array}{ll}
g_1 = \psi_{n1}(\psi_{n1}-1)+s_1\psi_{n1}+s_2-s_3n^2 & g_7 = \psi_{n1}(\psi_{n1}-1)+s_{13}\psi_{n1}+s_{14}-s_{15}n^2 \\
g_2 = \psi_{n2}(\psi_{n2}-1)+s_1\psi_{n2}+s_2-s_3n^2 & g_8 = \psi_{n2}(\psi_{n2}-1)+s_{13}\psi_{n2}+s_{14}-s_{15}n^2 \\
g_3 = in(s_4\psi_{n1}+s_5) & g_9 = in(s_{16}\psi_{n1}+s_{17}) \\
g_4 = in(s_4\psi_{n2}+s_5) & g_{10} = in(s_{16}\psi_{n2}+s_{17}) \\
g_5 = (s_6+s_7\zeta_{n1})A_{n1} & g_{11} = in\,s_{18}A_{n1} \\
g_6 = (s_6+s_7\zeta_{n2})A_{n2} & g_{12} = in\,s_{18}A_{n2}
\end{array}
\tag{A4}
$$

The constants in Eq. (23) are

$$
\begin{array}{ll}
L_1 = \dfrac{E_i}{(1+\upsilon)(1-2\upsilon)}r^{\beta_1-1} \qquad L_2 = \dfrac{E_i}{2(1+\upsilon)}r^{\beta_1-1} & K_7 = L_1\left[\left(1-\upsilon+\upsilon\psi_{0j}\right)G_{0j}-(1+\upsilon)\alpha_iA_{0j}\right] \\
K_1 = L_1\left[(1-\upsilon)\gamma_{0j}+\upsilon\right] & K_8 = L_1\left[(1-\upsilon)(inN_{nj}+1)+\upsilon\gamma_{nj}\right] \\
 & K_9 = L_1\left[(1-\upsilon)(inG_{n3}+G_{n1})+\upsilon\psi_{n1}G_{n1}-(1+\upsilon)\alpha_iA_{n1}\right] \\
K_2 = L_1\left[\left((1-\upsilon)\psi_{0j}+\upsilon\right)G_{0j}-(1+\upsilon)\alpha_iA_{0j}\right] & K_{10} = L_1\left[(1-\upsilon)(inG_{n4}+G_{n2})+\upsilon\psi_{n2}G_{n2}-(1+\upsilon)\alpha_iA_{n2}\right] \\
K_3 = L_1\left[(1-\upsilon)\gamma_{nj}+\upsilon(inN_{nj}+1)\right] & K_{11} = L_2\left[\gamma_{0j}-1\right] \\
K_4 = L_1\left[(1-\upsilon)\psi_{n1}G_{n1}+\upsilon(inG_{n3}+G_{n1})-(1+\upsilon)\alpha_iA_{n1}\right] & K_{12} = L_2\left[in+(\gamma_{nj}-1)N_{nj}\right] \\
K_5 = L_1\left[(1-\upsilon)\psi_{n2}G_{n2}+\upsilon(inG_{n4}+G_{n2})-(1+\upsilon)\alpha_iA_{n2}\right] & K_{13} = L_2\left[inG_{n1}+(\psi_{n1}-1)G_{n3}\right] \\
K_6 = L_1\left[1-\upsilon+\upsilon\gamma_{0j}\right] & K_{14} = L_2\left[inG_{n2}+(\psi_{n2}-1)G_{n4}\right]
\end{array}
\tag{A5}
$$

Appendix B

The coefficients in Eq. (29) are

$$
\begin{aligned}
&q_1 = \frac{3}{4} b_0 \left(n_0 - 1\right)\left(s_{11} - s_{10}\right) \frac{\sigma_\theta - \sigma_r}{\sigma_e} \frac{d\sigma_e}{dr} && q_5 = \frac{3}{2} b_0 \left(n_0 - 1\right) s_{20} \frac{\sigma_{r\theta}}{\sigma_e} \frac{d\sigma_e}{dr} \\
&q_2 = \frac{3}{4} b_0 \left(s_{11} - s_{10}\right)\left(\frac{d\sigma_\theta}{dr} - \frac{d\sigma_r}{dr}\right) && q_6 = \frac{3}{2} b_0 s_{20} \frac{d\sigma_{r\theta}}{dr} \\
&q_3 = \frac{3}{4} b_0 \left[\left(s_9 - s_8\right) + b_1\left(s_{11} - s_{10}\right)\right]\left(\sigma_\theta - \sigma_r\right) && q_7 = \frac{3}{2} b_0 \left(s_{19} + b_1 s_{20}\right)\sigma_{r\theta} \\
&q_4 = in \frac{3}{2} b_0 s_{12} \sigma_{r\theta} && q_8 = in \frac{3}{4} b_0 \left(s_{22} - s_{21}\right)\left(\sigma_\theta - \sigma_r\right)
\end{aligned}
\tag{A6}
$$

The parameters in Eq. (32) are

$$
\begin{aligned}
&h_1 = \left(b_1 + 2\right)\left(s_1 + b_1 + 1\right) + s_2 - n^2 s_3 && h_7 = \left(b_1 + 2\right)\left(s_{13} + b_1 + 1\right) + s_{14} - n^2 s_{15} \\
&h_2 = \left(b_1 + 1\right)\left(s_1 + b_1\right) + s_2 - n^2 s_3 && h_8 = \left(b_1 + 1\right)\left(s_{13} + b_1\right) + s_{14} - n^2 s_{15} \\
&h_3 = in\left(s_4 (b_1 + 2) + s_5\right) && h_9 = in\left(s_{16} (b_1 + 2) + s_{17}\right) \\
&h_4 = in\left(s_4 (b_1 + 1) + s_5\right) && h_{10} = in\left(s_{16} (b_1 + 1) + s_{17}\right) \\
&h_5 = \left(q_1 + q_2\right) {\sigma_e}^{n_0 - 1} && h_{11} = \left(q_5 + q_6\right) {\sigma_e}^{n_0 - 1} \\
&h_6 = \left(q_3 + q_4\right) {\sigma_e}^{n_0 - 1} && h_{12} = \left(q_7 + q_8\right) {\sigma_e}^{n_0 - 1}
\end{aligned}
\tag{A7}
$$

Stress rate components

$$
\begin{aligned}
\dot{\sigma}_r(r,\theta) = &\sum_{j=1}^{2} K_1 \left(C_{0j} + P_{0j}\right) r^{\gamma_{0j}} + \sum_{n=-\infty, n\neq 0}^{n=\infty} \Bigg\{ \sum_{j=1}^{4} K_3 C_{nj} r^{\gamma_{nj}} + L_1 \left[\left(\left(1-\upsilon\right)\left(b_1 + 1\right) + \upsilon\right) H_{n2} + in\upsilon H_{n4}\right] r^{b_1+1} \\
&+ L_1 \left[\left(\left(1-\upsilon\right)\left(b_1 + 2\right) + \upsilon\right) H_{n1} + in\upsilon H_{n3} + \left(1-\upsilon\right)\frac{dH_{n2}}{dr}\right] r^{b_1+2} + L_1 \left(1-\upsilon\right)\frac{dH_{n1}}{dr} r^{b_1+3} \Bigg\} e^{in\theta} - 2G \sum_{n=-\infty}^{+\infty} \dot{\varepsilon}^{c}_{r,n}(r)\, e^{in\theta} \\
\\
\dot{\sigma}_\theta(r,\theta) = &\sum_{j=1}^{2} K_6 \left(C_{0j} + P_{0j}\right) r^{\gamma_{0j}} + \sum_{n=-\infty, n\neq 0}^{n=\infty} \Bigg\{ \sum_{j=1}^{4} K_8 C_{nj} r^{\gamma_{nj}} + L_1 \left[\left(\upsilon\left(b_1 + 1\right) + 1 - \upsilon\right) H_{n2} + in\left(1-\upsilon\right) H_{n4}\right] r^{b_1+1} \\
&+ L_1 \left[\left(\upsilon\left(b_1 + 2\right) + 1 - \upsilon\right) H_{n1} + in\left(1-\upsilon\right) H_{n3} + \upsilon\frac{dH_{n2}}{dr}\right] r^{b_1+2} + L_1 \upsilon\frac{dH_{n1}}{dr} r^{b_1+3} \Bigg\} e^{in\theta} - 2G \sum_{n=-\infty}^{+\infty} \dot{\varepsilon}^{c}_{\theta,n}(r)\, e^{in\theta} \\
\\
\dot{\sigma}_{r\theta}(r,\theta) = &\sum_{j=1}^{2} K_{11} \left(C_{0j} + P_{0j}\right) r^{\gamma_{0j}} + \sum_{n=-\infty, n\neq 0}^{n=\infty} \Bigg\{ \sum_{j=1}^{4} K_{12} C_{nj} r^{\gamma_{nj}} + L_2 \left(inH_{n2} + b_1 H_{n4}\right) r^{b_1+1} \\
&+ L_2 \left[inH_{n1} + \left(b_1 + 1\right) H_{n3} + \frac{dH_{n4}}{dr}\right] r^{b_1+2} + L_2 \frac{dH_{n3}}{dr} r^{b_1+3} \Bigg\} e^{in\theta} - 2G \sum_{n=-\infty}^{+\infty} \dot{\varepsilon}^{c}_{r\theta,n}(r)\, e^{in\theta}
\end{aligned}
\tag{A8}
$$